DISSERTATIONES PHYSICAE UNIVERSITATIS TARTUENSIS
62

DISSERTATIONES PHYSICAE UNIVERSITATIS TARTUENSIS
62

VIGEN ISSAHHANJAN

Hole and interstitial centres in radiation-resistant MgO single crystals

TARTU UNIVERSITY
PRESS

This study was carried out at the Institute of Physics, University of Tartu.

The dissertation was admitted on September 5, 2008, in partial fulfilment of the requirements for the degree of Doctor of Philosophy in physics (solid state physics), and allowed to defence by the Council of the Institute of Physics, University of Tartu.

Supervisors: D.Sc. Tiit Kärner, Institute of Physics, University of Tartu, Estonia
D.Sc., Prof. Aleksandr Lushchik, Institute of Physics, University of Tartu, Estonia

Opponents: Dr phys. Anatoli Popov, The Institute of Solid State Physics, University of Latvia, Latvia

Defence: November 5, 2008 at the University of Tartu, Estonia

ISSN 1406–0647
ISBN 978–9949–11–969–1 (trükis)
ISBN 978–9949–11–970–7 (PDF)

Tartu Ülikooli Kirjastus
www.tyk.ee
Tellimuse nr 436

CONTENTS

2

LIST OF PUBLICATIONS

List of original papers included in this thesis:

I. S. A. Dolgov, V. Issahhanjan, T. Kärner, A. Maaroos, S. Nakonechnyi, "$V_{OH\text{-}Be}$ – a new and unusual member in the family of V centres", *J. Phys.: Condens. Matter*, 14, 8881–8888, 2002

II. S. A. Dolgov, V. Issahhanjan, T. Kärner, A. Maaroos, S. Nakonechnyi, "Electron paramagnetic resonance of the $[Be]^+$ centre in MgO:Be", *J. Phys.: Condens. Matter,* **15**, 6871–6878, 2003

III. T. Kärner, S. A. Dolgov, V. Issahhanjan, A. Maaroos, S. Nakonechnyi, "Paramagnetic centres in Be-doped MgO single crystals", *Rad. Eff. Def. Sol.*, **185**, 163–166, 2003

IV. S. A. Dolgov, V. Issahhanjan, T. Kärner, P. Liblik, A. Maaroos, S. Nakonechnyi, "Luminescence of $[Be]^+$ centre in MgO:Be", *Rad. Meas.*, **38**, 699–702, 2004

V. V. Issahhanjan, T. Kärner, A. Maaroos, S. Nakonechnyi, "Spin relaxation processes in the defect hole of Be-doped MgO single crystals", *Phys. Stat. Sol. (c)*, **2**, 426–429, 2005

VI. A. Lushchik, T. Kärner, Ch. Lushchik, E. Vasil'chenko, S. Dolgov, V. Issahhanjan, P. Liblik, "Dependence of long-lived defect creation on excitation density in MgO single crystals", *Phys. Stat. Sol. (c)*, **4 (3)**, 1084–1087, 2007

VII. A. Lushchik, Ch. Lushchik, K. Schwartz, E. Vasil'chenko, T. Kärner, I. Kudryavtseva, V. Issahhanjan, A. Shugai, "Stabilization and annealing of interstitials formed by radiation in binary metal oxides and fluorides", *Nucl. Instr. And Meth. B*, **266**, 2868–2871, 2008

Conference presentation:

- S. A. Dolgov, V. Issahhanjan, T. Kärner, A. Maaroos, S. Nakonechnyi, "$Be^{2+}O^-$ centre in Be-doped MgO single crystals," *5th European Conference on Luminescent Detectors and Transformers of Ionizing Radiation (LUMDETR-2003*), Prague, Czech Republic, September 1–5, 2003 (poster).
- V. Issahhanjan, T. Kärner, A. Maaroos, S. Nakonechnyi, "Spin relaxation processes in the hole centres of Be-doped MgO single crystals", *15th International Conference on Defects in Insulating Materials ICDIM2004*, Riga, Latvia, July 11–16, 2004 (poster)

- V. Issahhanjan, T. Kärner, A. Maaroos, S. Nakonechnyi, "VOH-Be and [Be]+ hole centres in the Be-doped MgO single crystals", *Radiation Effects in Solids Workshop*, Erice, Italy, July 17–29, 2004 (poster)
- A. Lushchik, T. Kärner, Ch. Lushchik, E. Vasil'chenko, S. Dolgov, V. Issahhanjan, P. Liblik, "Dependence of long-lived defect creation on excitation density in LiF, MgO and SiO_2," *10^{th} Europhysical Conference on Defects in Insulating Materials (EURODIM-2006)*, Milano, Italy, July 10–14, 2006 (oral)
- A. Lushchik, Ch. Lushchik, K. Schwartz, E. Vasil'chenko, T. Kärner, I. Kudryavtseva, V. Issahhanjan, A. Shugai, "Stabilization and annealing of interstitials formed by radiation in binary metal oxides and fluorides," *14^{th} International Conference on Radiation Effects in Insulators (REI-2007),* Caen, France, August 28 – September 1, 2007 (oral)
- A. Lushchik, Ch. Lushchik, V. Issahhanjan, T. Kärner, P. Liblik, A. Maaroos, A. Shugai, E. Vasil'chenko, "Contribution of hot electron-hole recombination into radiation damage of wide-gap materials for nuclear energetics and other applications," *International Baltic Sea Region conference "Functional materials and nanotechnologies,"* Riga, April 1–4, 2008 (oral).

The author's contribution:

The author has performed EPR measurements and an experimental data analysis. A new EPR simulation software "VirtualEPR Spectrometer" was created and used in the data analysis. Main conclusions were made in cooperation with the supervisors of the author.

ABBREVIATIONS

CB	Conduction band
CL	Cathodoluminescence
EPR	Electron paramagnetic resonance
DFT	Density functional theory
EVI	Electron vibration interaction
GGA	Generalized-gradient approximation
GWA	GW approximation
HF	Hyperfine
LDA	Local density approximation
MgO	Magnesium oxide
RT	Room temperature
SH	Spin-Hamiltonian
SHF	Superhyperfine
SHI	Swift heavy ions
SLC	Spin-lattice coupling
SSC	Spin-spin coupling
TL	Thermoluminescence
VB	Valence band

3

I. INTRODUCTION

The recent global energetic crisis has stimulated investigations related to new sources of energy. One of the few possible solutions with a potential to satisfy the ever increasing global demand is thermonuclear fusion. Several technological problems are standing on the way to commercializing fusion reactors. One of such problems is the presence of a significant radiation field consisting of high energy neutron and gamma radiation fluxes, extending well beyond the first wall of the reactor [1]. The materials behind this relatively thin protection can be divided into 4 categories:

- Structural materials (mainly steels) with thermo-mechanical properties of a concern
- Superconductors and organic insulation for coils (far away from radiation source)
- Li-containing blanket materials for tritium production and heat extraction ($LiAlO_2$, Li_2SiO_3, $LiBeF_3$)
- Insulating materials for use in heating and current drive, diagnostics systems, and protection (BeO, MgO, Al_2O_3, $MgAl_2O_4$, SiO_2)

The latter point brought gave an idea to present a possibly full insight into the hole and interstitial centres in radiation-resistant magnesium oxide single crystals. During this work, pure and Be-doped MgO single crystals were investigated by means of EPR, electron paramagnetic resonance (EPR), cathodoluminescence (CL), and thermoluminescence (TL). The formation of hole and interstitial centres was examined under different types of irradiation. The crystals were subject to γ-rays, X-rays, neutron and swift heavy ion irradiations at different temperatures.

The investigation of MgO:Be single crystals has several advantages in comparison to other doped MgO crystals (MgO:Na, MgO:Li, MgO:Ge etc.), which are:

1. Be and Mg are isoelectronic, which means that, in the first approximation, the Columbic forces can be neglected in defect formation
2. Hole trapping in MgO:Be is similar to self-trapping in pure MgO crystals (due to the 1st point)
3. The two discovered paramagnetic trapped-hole centres [I – V] with very different structures contribute to the understanding of hole centre properties
4. The small size and non-zero nuclear spin of Be makes it a certain spin label in oxide materials.

The comparison of different types of trapped-hole centres in pure and doped MgO crystals was made in light of presumable $[Ca]^+$ centre and hole self-trapping in pure MgO.

Our results also confirmed the existence of a novel non-impact mechanism of formation of stable interstitials in MgO single crystals in addition to a well-known knock-out mechanism [VI–VII], namely the formation of stable interstitial centres was due to recombination of hot charge carriers (holes and electrons) with an energy release exceeding the energy of Frenkel defect pair creation. The hot charge carriers were created due to electronic excitations in the tracks of swift heavy ions by which the MgO crystals were irradiated.

This thesis is divided into 3 parts, apart from the introductory part. In the first part of this thesis, a short theoretical background of electron paramagnetic resonance (EPR) and spin relaxation processes is given.

The second part contains an overview of a variety of discovered trapped-hole centres in pure and doped MgO single crystals. We report two new paramagnetic trapped-hole centres discovered in MgO:Be single crystals. Their physical properties along with the used experimental and theoretical methodologies are given. A comparison of above mentioned centres is presented.

The third chapter sheds light on interstitial centres in MgO single crystals. The EPR spectra, parameters and thermal stability of these centres are given. A novel non-impact mechanism of formation of stable interstitials is described with supporting experimental evidences.

The summary highlights the main results and conclusions of this thesis.

2. THEORETICAL BACKGROUND

2.1. Electron Paramagnetic Resonance

The method of Electron Paramagnetic Resonance was evolved from the Stern-Gerlah experiment in 1922, where they showed that electrons can have two possible orientations of the magnetic moment. Since in the experiment the angular momentum of electrons was zero, in 1925 Goudsmit and Uhlenbeck postulated that the electrons had an intrinsic angular momentum independent of its orbital characteristic which was called *electron spin* [2].

In the EPR experiments applied static magnetic field B_0 aligns the magnetic moment of an electron either parallel ($M_S = -1/2$) or anti-parallel ($M_S = +1/2$) to the field direction removing spin degeneracy of the energy level. This effect is called the Zeeman effect and it corresponds to the Stark effect in the electric field. The energy difference between these levels is given by formula

$$\Delta E = \Delta M_S g \mu_B B_0, \tag{1}$$

where $\Delta M_S = 1$ is the difference between parallel and antiparallel moment orientations, g – so-called electron's g-factor, μ_B – Bohr's magneton, B_0 – static magnetic field. In order to move the electron between these energy levels by either emitting or absorbing the energy ΔE, an electromagnetic field $\Delta E = h\nu$ must be applied. By varying the static magnetic field B_0 with constant electromagnetic field frequency ν, or vice versa, an absorption peak is detected. Subsequently, from equation (1) the g-factor can be calculated, which characterizes the electron spin. For the free electron system, g-factor is $g_e = 2.0023$.

2.2. Spin-Hamiltonian

Quantum physics uses operator notation to describe the EPR energy transitions, the so-called Spin-Hamiltonian (SH). Subsequently, most of the paramagnetic systems can be described with the following SH:

$$\hat{H} = \beta_B \hat{\mathbf{S}} \mathbf{g} \vec{\mathbf{B}} + h \hat{\mathbf{S}} \mathbf{D} \hat{\mathbf{S}} + \sum_i (h \hat{\mathbf{S}} \mathbf{A}_i \hat{\mathbf{I}}_i - g_N \beta_N \vec{\mathbf{B}} \hat{\mathbf{I}}_i + h \hat{\mathbf{I}}_i \mathbf{Q}_i \hat{\mathbf{I}}_i), \tag{2}$$

where $\beta_B = 9.27 \cdot 10^{-24}$ J/T is Bohr's magneton, $\beta_N = 5.05 \cdot 10^{-27}$ J/T is nuclear magneton, $h = 6.62 \cdot 10^{-34}$ J·s is Plank's constant, $\mathbf{g}$ – electron g-factor tensor, $\vec{\mathbf{B}}$ – static magnetic field vector, $\hat{\mathbf{S}}$ – electron spin operator, $\mathbf{D}$ – quadrupole interaction tensor between electron spin and crystal field (for $S \geq 1$), g_N – nuclear spin, $\hat{\mathbf{I}}_i$ – nuclear spin operator, $\mathbf{A}_i$

– (super)hyperfine interaction tensor between electron and nuclear spins, $\mathbf{Q}_i$ – quadrupole interaction tensor between nuclear spin and crystal field (for I ≥ 1), summation is done over all nuclear spins. SH forms a matrix of size $(2S+1)\prod_i (2I_i+1)$, where S is the total electron spin, I_i – nuclear spin. The eigenvalues of the SH matrix represent the energy levels of the system under a static magnetic field, while eigenvectors are coefficients of overlapping of wave functions which can give the relative intensities of the EPR absorption lines.

In this thesis mostly tetragonal symmetry defects are under consideration. Moreover, all the experimental data are presented for the case when static magnetic field is along the MgO <100> principal axis, that is taken as the Z axis. In this case, only the perpendicular and parallel components of the g-factor tensor are distinguished: $g_\perp = g_x = g_y$ and $g_\parallel = g_z$.

2.2.1. g-Factor

The electron g-factor characterizes the type of the centre and some of its properties. In pure spin systems, the electron g-factor is always equal to the free-electron g-factor g_e. In real crystals, spin-orbital coupling must be considered, the influence of which can be evaluated using

$$\mathbf{g} = g_e \mathbf{1} + 2\lambda \mathbf{\Lambda}, \tag{3}$$

where **g** is an electron[1] g-factor tensor, g_e = 2.0023 – free electron g-factor, λ – spin-orbital coupling parameter, **Λ** – is a tensor which includes only assets from orbital moments of the excited states of the paramagnetic ion [2]. In a crystal field with tetragonal symmetry and the main symmetry axis taken as Z axis, only diagonal components of **Λ** will be non-zero with $\Lambda_z = 0$. Considering the *p*-states of the electron, in the first approximation the g-factor tensor components are given with the following [3]:

$$g_\perp = g_e - \frac{2\lambda}{\delta}, \tag{4a}$$

$$g_\parallel = g_e, \tag{4b}$$

where δ is the separation between the excited $p_{x,y}$ and p_z states of the paramagnetic ion. Formula (4a) is important in identifying the type of the centre: as λ is negative for the holes and positive for the electrons, positive shift of $g_\perp$ from the free electron g-factor defines a hole centre,

[1] The results applied here are same for both electrons and holes

while negative shift defines an electron centre.

Value δ was initially connected to the optical absorption of the defect, but in [4] it was shown that taken the experimental values for g-factor shift and absorption band position gave an enormously high value for the spin-orbital coupling parameter λ. According to Schirmer et al. [5, 6] and Norget et al. [7], the value of δ is due to the intrapolaron transitions between the energy levels of the paramagnetic ion, which are forbidden: these transitions can still be registered in the absorption spectrum, but have a very low intensity. The optical absorption can be produced by both intrapolaron transitions between the allowed energy levels of the paramagnetic ion (giving a much higher energy for optical absorption) and interpolaron transitions between a paramagnetic ion and its ligands, i.e. electron transfer from a paramagnetic ion to the neighbouring ions under excitation.

The parallel g-factor shift $\Delta g_{\|} = g_{\|} - g_e$ is not zero in majority of the experimental data. The experimental value then shows the perturbation to the spin-orbital transitions from the neighbouring ions that allows the electron transfer to these ions with some probability. In [3] it was shown that the ratio between perpendicular $\Delta g_{\perp} = g_{\perp} - g_e$ and the parallel $\Delta g_{\|}$ g-factor shifts gives the approximate probability of such transfers. This probability can be used for describing the motion averaging of the EPR spectrum due to electron delocalization between equivalent neighbour ions.

2.2.2. Hyperfine interaction tensor

The interaction between the electrons and every nucleus in the defect is described by the HF tensor **A** which can be split into the isotropic *a* and anisotropic *b* terms. The isotropic interaction is due to the non-zero radial density of the electron wave function at the nucleus. It is known that only s-orbital electrons have non-zero probability to be at the nucleus and be a cause for the isotropic HF interaction. For the one-electron systems, Fermi showed [2] that isotropic term can be calculated using

$$a = \frac{2\mu_0}{3}\frac{g_e\beta\beta_N g_N}{h}\left|\psi(0)\right|^2 Hz, \qquad (5a)$$

where μ_0 is the magnetic constant, I_N – nucleus spin, g_N – nucleus g-factor (scalar), $|\psi(0)|^2$ – density of an electron wave function on a particular nucleus. With a known experimental value, one can subsequently estimate the probability of finding the particle on the particular nucleus.

The anisotropic term is due to the magnetic dipole-dipole interaction between an electron and nucleus. For the p-orbital electrons, in the point-dipole approximation this term can be evaluated with

$$b = \frac{2}{5}\frac{\mu_0}{4\pi}\frac{g_e \beta \beta_N g_N}{h}\left(\frac{1}{l^3} - \frac{6}{5}\frac{\langle \rho^2 \rangle}{l^5}\right) Hz, \qquad (5b)$$

where l – distance between nucleus and the paramagnetic ion, $\langle \rho^2 \rangle$ describes the radial extent of the wave function.

In general, from the EPR experiment the diagonal SHF tensor parameters are measured, i.e. A_x, A_y and A_z. Using transformation from the defect coordinate system (CS) to crystal CS, the SHF tensor is calculated. In the case of tetragonal symmetry defects, only perpendicular and parallel components are distinguished in the SHF tensor: $A_\perp = A_x = A_y$ and $A_\parallel = A_z$. From the experiment, these terms can be calculated using

$$a = \frac{A_x + A_y + c \cdot A_z}{2 + c} Hz, \qquad (6a)$$

$$b = \frac{c \cdot A_z - \frac{A_x + A_y}{2}}{2 + c} Hz, \qquad (6b)$$

where c is the coefficient depending on the g-factor shift: $c = 1 + \left(\Delta g_x + \Delta g_y\right)/4 = 1 + \Delta g_\perp / 2$. The experimental value for isotropic hyperfine interaction a shows the admixture of the nucleus wave function to the paramagnetic ion wave function, while parameter b can give an estimate for the distance l between a paramagnetic ion and nucleus, hence, describing the entire defect structure.

2.2.3. Spin relaxation mechanisms

The relaxation of the excited spin to the ground state depends on 2 different interactions of the spin with its surroundings. One of those is spin-spin coupling (SSC) which causes an inhomogeneous broadening of the EPR absorption band. SSC is caused by different mechanisms of magnetic interactions of the surrounding ions (magnetic dipole interaction, resonance induced transitions) which are inhomogeneously broadening the EPR absorption linewidth. In general, calculation of the spin-spin relaxation time is too complex, although based on experimental data estimation is possible using $\tau_2 = 1/(2\gamma \Delta B)$, where ΔB is the absorption band linewidth.

Another mechanism of spin relaxation is caused by electron vibration interactions (EVI). Such interactions influence the electron spin indirectly, via the spin-orbital coupling. The spin relaxations due to EVI are called the spin-lattice coupling (SLC). SLC causes a homogenous line broadening of the EPR absorption band. The theory of SLC was developed by Kronig and van Fleck [8], and this relaxation mechanism is called also *Kronig-van Fleck mechanism*. The SLC relaxation time can be given with the following formula:

$$\tau_1(T) = \left(a \cot\left(\frac{h\upsilon}{2kT}\right) + bT_0^n + \frac{c}{\exp\left(\frac{\Delta}{kT}\right) - 1} \right)^{-1}, \qquad (7)$$

where T is the temperature, ν – induced microwave frequency, k – Boltzmann constant, a, b, c, and n– fitting coefficients that depend on a particular spin system. The meanings of terms in the denominator are as follows:

- The first term describe the direct single phonon process
- The second term describes the Raman process with n defining the multiplicity of the transition
- The Orbach process which consists of a direct excitation to an energy Δ following an indirect relaxation

Knowing the spin-spin and spin-lattice relaxation time, the EPR absorption linewidth (full width at half maximum) can be calculated with the following formula:

$$\Delta B_{FWHM} = \frac{1}{2\tau_1} + \frac{\sqrt{1 + \gamma^2 B_1^2 \tau_1 \tau_2}}{\gamma \tau_2}, \qquad (8)$$

where τ_1 and τ_2 are the spin-lattice and spin-spin relaxation times, respectively, γ – gyroscopic constant, B_1 – microwave magnetic component. The intensity of the absorption band can be given with

$$I = \frac{2\pi\upsilon \cdot S(S+1) \cdot B_1 \tau_2}{T(1 + \gamma^2 B_1^2 \tau_1 \tau_2)}, \qquad (9)$$

where, in addition to known parameters, the electron spin S was added.

3. TRAPPED-HOLE CENTRES

Even very pure MgO crystals have natural aliovalent impurities, like H^+, F^-, Al^{3+}, Si^{4+}, Fe^{3+} [9]. They appear already in the starting powder used for crystal growth. Various impurities have also been intentionally introduced into the crystals by doping, like isovalent Be^{2+}, Ca^{2+}, and aliovalent Li^+, Na^+, K^+, Ge^{4+} etc.. The net charge of these impurities is partially compensated by cation vacancies which appear during crystal growth. It is only the existing vacancies that cause the formation of trapped-hole centres. There are two different mechanisms for that: one is the valence-compensation of aliovalent impurities, and the other is an increase of the potential well depth by isovalent impurities due to local lattice deformation. In both cases, the holes are trapped by oxygen ions next to cation vacancy.

Before moving on with trapped-hole centres there is a strong need for an overview of some general physical and electronic properties of MgO.

3.1. Physical properties and electron structure of MgO

Magnesium oxide is a wide-gap alkaline earth metal oxide that occurs naturally as a periclase. MgO powder is easily made by burning magnesium ribbon that oxidizes in a bright white light. The produced powder is used for MgO crystal growth.

A pure MgO crystal has a rocksalt type structure (Fig. 1), which is a cubic face-centred Bravais lattice, and belongs to space group O_h^5, (Fm3m, No. 225). Some physical properties of the crystal are presented in Table 1. MgO has a high fraction ionic character $f_i = 0.84$ and net cation charge q(Mg) ≈ 1.95 [13]. The ionic radius of 6-coordinated Mg^{2+} is $r_c = 0.72$ A, while a 6-coordinated oxygen ion O^{2-} has $r_a = 1.40$ Å [14]. The radii ratio $r_a/r_c = 0.51$ shows that oxygen ions create almost

Table 1. Physical properties of a MgO crystal

Parameter	Value
Lattice constant, a_0	4.212 Å [10]
Density, ρ	3650 kg/m^3
Melting temperature, T_m	2800 °C
Low frequency dielectric constant, ε_0	9.86 [11]
High frequency dielectric constant, ε_∞	2.9565 [11]
Transverse optic phonon, ω_{TO}	400 cm^{-1} [12]
Longitude optic phonon, ω_{LO}	721 cm^{-1} [12]

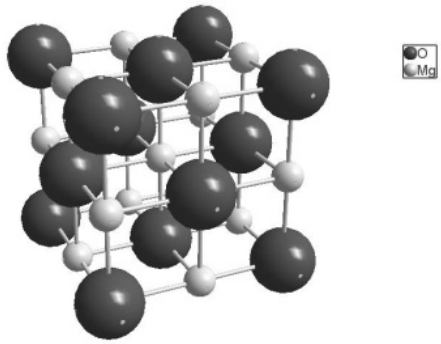

Figure 1. MgO Bravais lattice. Ion space filling is reduced for illustrative purposes**.**

octahedral close anion packing with magnesium cation filling the octahedral interstices.

MgO is a dielectric with a band gap E_g = 7.83 eV [15]. Fig. 2 shows the reflectance spectrum of MgO crystals with a theoretical separation to exciton and interband transition. A detailed exciton reflectance spectrum at 25 K is shown in Fig. 3 [16]. Two doublets can be observed in the spectrum. The peaks of the first doublet at $E_{\Gamma 1}$ = 7.689 eV and $E_{\Gamma 2}$ = 7.715 eV are due to spin-orbit-split Γ exciton, while those of the second doublet at E_{EPC1} = 7.752 eV and E_{EPC2} = 7.768 eV are due to the spin-orbit-split exciton-phonon complex.

Different calculations of energy bands for a MgO crystal were performed using the Density Functional Theory (DFT) using a variety of functionals based on approximations, like local-density (LDA), generalized-gradient (GGA), so-called GW approximation (GWA). The latter gives the best results for the electron excited states with the best energy gap approximation and band structure [17] which are present in Fig. 4. Here the band structure is calculated along the ΓX and ΓL symmetry points. It can be seen that both calculations predict a direct interband transition in Γ point with GWA method predicted band gap E_g = 7.7 eV which is very close to the experimental value. The bottom of the

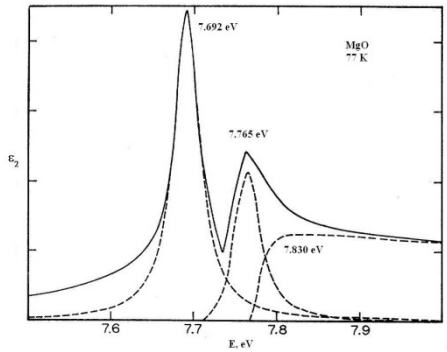

Figure 2. MgO reflectance spectrum at 77 K. The solid line shows the experimental data. The Dashed lines denote possible separation into an exciton and interband transition.

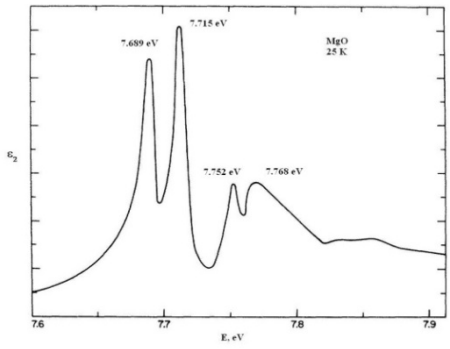

Figure 3. Reflectance spectrum of the MgO exciton doublet in the MgO reflectance spectrum at 25 K. There are two doublets due to spin-orbit-split Γ and EPC/excitons.

conduction band (CB) is formed by a Mg 3s band, while the top of the valence band (VB) consists of an oxygen 2p band. There is a strong hybridization between O and Mg orbital in both the valence and conduction bands.

The measurements of the VB width gives a wide spectrum of values from 3.3 eV (EMS) to 8.5 eV (X-ray emission) [18], with an even wider spectrum of the calculated values. The valence band width is approximately E_v = 5 eV, which lies between the experimental values.

3.2. V-centres

The holes trapped next to cation vacancies are called V-type centres. All natural impurity centres in MgO are of the V-type. The first report on trapped-hole centres in MgO was by Wertz et al. on X-irradiated single crystals [19, 20] during an EPR experiment at 77 K. With a static magnetic field **B** at an arbitrary angle with respect to the principal <100> axis, a set of three lines was observed. When magnetic field **B** is parallel to <100> axis, two lines with $g_\perp$ = 2.0386 and $g_\parallel$ = 2.0033 can be observed on the EPR spectrum (Fig. 5). The intensity of the perpendicular component is almost twice as high as that of the parallel. The spectrum observation is consistent with a defect with tetragonal symmetry about the <100> axis. The ENDOR spectra of such crystals [20] showed a small hyperfine (HF) splitting of the perpendicular group of lines consistent with the interaction between spin S = 1/2 and nuclear spin I = 5/2. Spin S = 1/2 is obviously a trapped hole as there is a positive deviation of the g-factor from the free electron value. The nucleus spin was identified as Al^{27} isotope. The centre was named V_{Al} with the

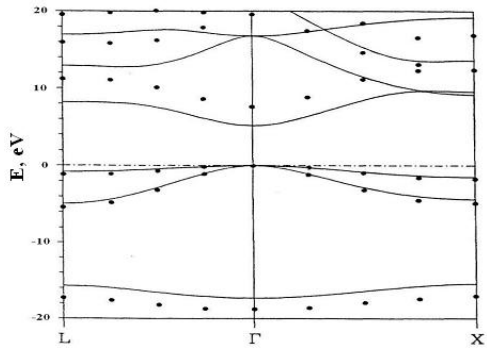

Figure 4. Energy bands of MgO calculated using LDA approximation (solid lines) and GW approximation (dotted lines).

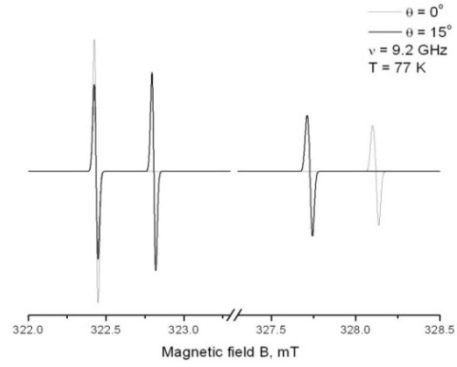

Figure 5. EPR spectrum of V_{al} centre in a pure MgO crystal. θ is an angle between the static magnetic field and <100> principal axis. The spectrum is simulated using VirtualEPR Spectrometer software.

Table 2. Parameters of V_{Al}, V_{OH}, V^-, and V^0 centres.

	$g_\perp$	$g_\parallel$	$A_\perp$, *MHz*	$A_\parallel$, *MHz*	*a, MHz*	*b, MHz*
V_{Al}	2,0386	2,0033	-0,073	0,176	0,011	0,083
V^-	2,0386	2,0033				
V_{OH}	2,0398	2,0033	-2,315	4,843	0,101	2,371
V^0	2,0395	2,0033				

following structure: $O^- - v_c - O^{2-} - Al^{3+}$ (hole trapped on an oxygen ion interacting with Al^{27} isotope). The parameters of V_{Al} centre along with SHF splitting are presented in Tab. 2. In the optical absorption spectrum the presence of V_{Al} centre manifests itself in the absorption band at 2.3 eV [20]. The temperature of thermal destruction of V_{Al} centre is 370 K [21].

Another group of V-type centres can be observed in the MgO crystals grown in the presence of moisture, the so-called MgO:OH crystals. One can still observe the V_{Al} centre in these crystals along with V_{OH}, V^- and V^0 centres. These centres can be formed only from the so-called V_{OH}^- centre (cation vacancy occupied by proton $O^{2-} - v_c - OH^-$). The V_{OH}^- centre can be formed by heating of a MgO:OH crystal to the temperatures above 1200 K, followed by quenching to room temperature. This centre is not paramagnetic and cannot be observed using the EPR method, but it still can be monitored with the infrared absorption band at 0.4 eV. In [22], a MgO:OH crystal was subjected to gamma irradiation at T = 77 K which created a new optical absorption band at 2.21 eV and in the EPR spectrum. This centre is formed from the V_{OH}^- centre by a hole capture on the oxygen ion adjacent to a proton: V_{OH} centre with a structure $O^- - v_c - OH^-$ [23]. The centre has a tetragonal symmetry along <100> axis with g-factor $g_\perp = 2.0398$ and $g_\parallel = 2.0033$ (Tab. 2). This centre is not stable at room temperature (half-life is of order of hours) annealing to a somewhat more stable V_{Al} centre (half-life is of order of days). The temperature of its thermal destruction is 335 K [21].

A different crystal coloration can be produced by electron irradiation with a dose of $\sim 10^{17}$ e/cm^2 [23]. Another optical absorption band is subsequently formed at 2.33 eV [24]. Using the EPR method, one can observe three absorption bands when a static magnetic field is at an arbitrary angle with respect to <100> axis (Fig. 6). The centre has same g-factor as V_{Al} centre $g_\perp = 2.0386$ and $g_\parallel = 2.0033$ (Tab. 2), but has no SHF splitting which can be observed by a more precise ENDOR spectrum. The centre was named V^- and has the following structure: $O^{2-} - v_c - O^-$. Due to the negative net charge of the centre, the depth of the

local potential well is increased which renders the centre very stable: the half-life is of order of years and the thermal destruction temperature at 420 K [21].

Along with the V^- centre, another paramagnetic centre can be observed during irradiation at reduced temperatures with S = 1 (Fig. 6). This new centre, which is called V^0, is formed from the V^- centre by a hole capture on the adjacent to cation vacancy O^{2-} ion: $O^- - v_c - O^-$. The centre has a tetragonal symmetry along the <100> type axis. Its g-factor is $g_\perp$ = 2.0395 and $g_\parallel$ = 2.0033 (Tab. 2). In the absorption spectrum the band at 2.36 eV is associated with this centre [25]. A V^0 centre is very unstable at the room temperature and degrades quite quickly to a V^- centre (Fig. 7), with the total sum of the number of these centres staying almost constant.

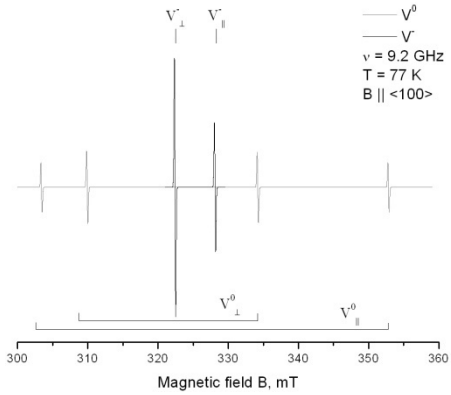

Figure 7. EPR spectrum of V^- and V^0 centres in a MgO crystal grown in moisture. The static magnetic field is parallel to the <100> axis. The Spectrum is simulated using the VirtualEPR Spectrometer software.

The mechanism of the V^- centre formation under irradiation is worth mentioning. In [23] it is described in the following way:

$$V_{OH}^- + e^+ \rightarrow V_{OH} \rightarrow V^- + H^+,$$

i.e. a hole trapped by a V_{OH}^- centre produces a V_{OH} centre which decays to the V^- and H^+ centers. At the same time, Kärner et al. have introduced another formation mechanism [21, 26]:

$$V_{OH}^- + e^+ \rightarrow V_{OH};\ V_{OH} + e^- \rightarrow V_{OH}^{-*} \rightarrow V^- + H^0,$$

namely, first a hole is trapped by a V_{OH}^- centre forming a V_{OH} centre, which under irradiation captures an electron in the excited state. The latter recombines with a trapped-hole producing hydrogen and V^- centre. This was shown in [26] by MgO:OH crystals irradiation at temperatures T = 295 K, 315 K, 400 K and 500 K. The ratio between V^- and V_{OH} EPR line intensities was measured. A rapid growth of this

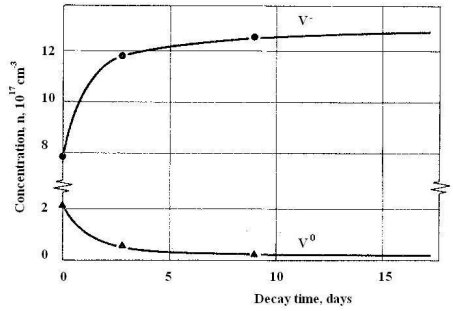

Figure 6. Increase of the concentration of V^- and decay of V^0 centres in MgO:OH crystal at room temperature.

ratio was detected only when irradiation was performed at RT. A very small growth was observable at 315 K at low doses and it showed zero growth when the dose increased. For the temperatures higher than that of the thermal destruction of V_{OH} centre (T = 335 K), there was no growth at all, proving that a V^- centre can be formed only from the existing V_{OH} centres which proves the latter formation mechanism.

3.3. Lithium and sodium containing hole centres

Impurities such as H, F, Al, Si and Fe are ubiquitous in the starting powders used in MgO crystal growth. At the same time, a variety of impurities have been intentionally introduced in a MgO crystal by either doping or diffusion. Impurities could be as aliovalent, like Li, Na, as isovalent, like Be, Ca. Here we will discuss singly charged Li and Na impurities.

During crystal growth, Li^+ and Na^+ ions substitute Mg^{2+} cation creating perturbed negatively charged vacancies which are referred to as $[Li]^-$ and $[Na]^-$, respectively [4]. These defects are not paramagnetic or optically active. After gamma or electron irradiation at 77 K, a hole is trapped on these centres forming neutral paramagnetic $[Li]^0$ and $[Na]^0$ centres, respectively [18].

The EPR spectrum of both centres is presented in Fig. 8. With static magnetic field B parallel to <100> type axis of the MgO crystal, a group of four overlapping lines can be observed on the left side of both spectra (perpendicular components), which is SHF interaction between nucleus I = 3/2 and spin S = 1/2. Both centres have a tetragonal symmetry along the <100> type axis with structures of $Li^+ - O^-$ and $Na^+ - O^-$, respectively.

The g-factor for $[Li]^0$ centre is $g_\perp$ = 2.0545 and $g_\parallel$ = 2.0049 was obtained from the ENDOR experiment in [3, 4]. An optical absorption band for $[Li]^0$ centre is observed at 1.83 eV. The centre shows a different stability for different formation mechanisms [27]. For the crystals quenched from 1500 K or irradiated with doses of ~$5 \cdot 10^{18}$ e/cm^2 at room temperature the centre is stable even at temperatures

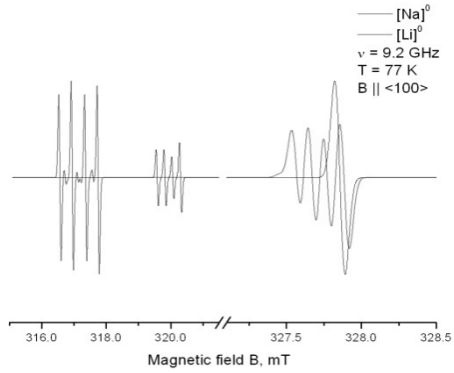

Figure 8. EPR spectra of $[Li]^0$ and $[Na]^0$ centres. The static magnetic field is parallel to the <100> axis. The spectrum is simulated using the VirtualEPR Spectrometer software.

Table 3. Parameters of $[Li]^0$ and $[Na]^0$ centres

	$g_\perp$	$g_{\|\|}$	$A_\perp$, MHz	$A_{\|\|}$, MHz	a, MHz	b, MHz
$[Li]^0$	2,0545	2,0049	-6,912	0,087	-4,539	2,313
$[Na]^0$	2,0725	2,0057	-11,259	3,024	-6,388	4,706

T >> 295 K. At the same time, the crystals irradiated with a short ionizing dose of electrons at 80 K are destroyed by the thermal release of a hole at T_{Li} = 230 K [21]. This difference is explained in [9]: at normal crystal growth conditions Li^+ ions are concentrated primarily in the precipitates, randomly distributed in the crystal. At high temperatures or upon extensive irradiation these precipitates give rise to a localized lithium rich environment surrounding the precipitate, the so-called *microgalaxy*. Due to the charge neutrality, a hole is captured on the neighbouring oxygen ions giving rise to $[Li]^0$ centres. These holes are stable in the microgalaxy because the loss of a few holes will result in the negative charge of microgalaxy that will impede a further loss of the holes.

Although $[Na]^0$ centre has the same structure as $[Li]^0$, their properties differ significantly. Its g-factor $g_\perp$ = 2.0725 and $g_{||}$ = 2.0057 (Tab. 3) have much bigger shifts from the free-electron g-factor compared to the ones of $[Li]^0$ centre. This is manifested in ~1.4 times decrease in the difference between the ground and first excited states of the hole ΔE = 1.34 eV. $[Na]^0$ centre is different from the other so far described trapped-hole centres in that its parallel component of SHF tensor $A_{||}$ = 3.024 MHz is quite big, which produces another group of four lines on the right side of the spectrum. The temperature of the thermal destruction of the centre is T_{Na} = 190 K [28].

3.4. Beryllium containing centres

The MgO:Be single crystals were grown at the Institute of Physics, University of Tartu, by a variation of the arc fusion technique [29] using an arc furnace with two carefully cleaned spectrographic-grade graphite electrodes. The starting material was a mixture of high-purity MgO and BeO. The mixture was stirred, heated 1 h at ~1520 K to remove moisture and chemisorbed water and decompose any unwanted Be compounds, and compressed. Taking into account that at the temperature of crystal growth (~3075 K) a rapid evaporation of BeO was expected, the concentration of BeO in the starting powder was taken as 2000 ppm, that is, twice as high as the greatest substitutional solubility of Be ions in MgO given in the literature [30, 31]. As a result, crystals of up to

$15\times15\times10$ mm^3 were formed. The average content of the most common transition metal impurities in these crystals was about 10 ppm.

In MgO, Be^{2+} substitutes the Mg^{2+} ion and was found to be present both in the form of isolated ions and within defect complexes. In the first case, under irradiation it was able to trap both electrons and holes, forming Be^{1+} and $Be^{2+} - O^-$ centres, respectively. The estimated content of Be in the MgO:Be crystals was about 100 ppm. The grown crystals were cloudy that is a characteristic of high a hydrogen concentration.

The EPR spectra of the MgO:Be crystal were measured with an X-band (9.928 GHz) ERS 231 spectrometer. A continuous-flow helium cryostat (Oxford Instruments, ESR900) was used to keep the samples at the necessary temperature. Pulse annealing of the samples was carried out to determine the thermal stability of the observed EPR-active centre. Upon pulse annealing, the crystals were kept, after a fast heating, at the required temperature for 2 min and then cooled down to the measurement temperature. The optical absorption was measured using a Jasco V-550 spectrophotometer. The measured EPR spectra were analyzed using the computer programs VirtualEPR Spectrometer (University of Tartu, 2004), created by the author, and EPRNMR (Department of Chemistry, University of Saskatchewan, Canada, 1993).

3.4.1. $[Be]^+$ centre

3.4.1.1. Experimental results

After x-irradiation of MgO:Be single crystals at 77 K, a new paramagnetic centre is formed [II, III]. The EPR spectrum of this centre can be followed in the temperature range of 4 to 40 K and can be best observed at 4 K and at high microwave powers (> 1 mW) when signals from other centres are already saturated. At an arbitrary angle of magnetic field **B** with respect to the MgO principal <100> axis, EPR spectrum consists of four groups of lines which coincide

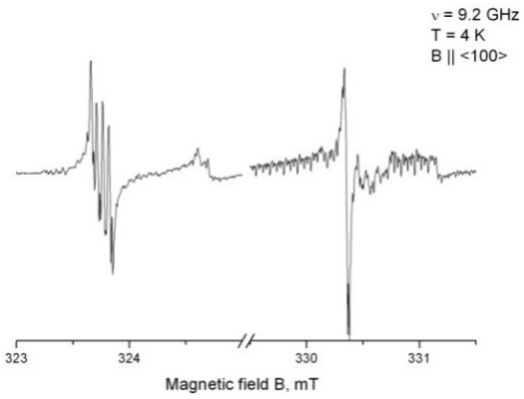

Figure 9. Experimental EPR spectrum of [Be]+ centre in MgO:Be at 4 K. The static magnetic field is parallel to the MgO <100> type axis.

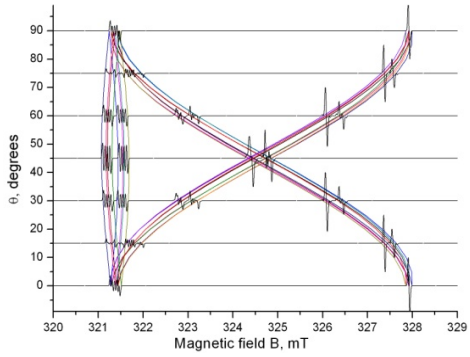

Figure 10. Roadmap of $[Be]^+$ with angle θ between the magnetic field and <100> principal axis in {100} type plane. Roadmap is calculated using the EPRNMR software. The EPR spectra are simulated using the VirtualEPR Spectrometer.

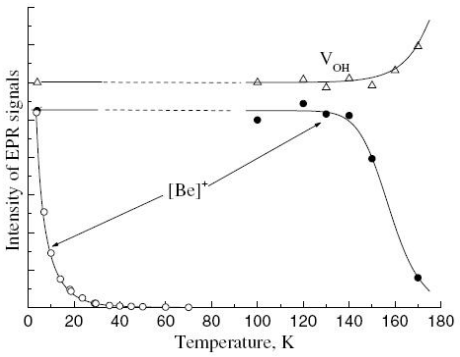

Figure 11. The temperature dependence of the intensity of the $[Be]^+$ EPR spectrum (open circles) and the isochronal annealing of the EPR signals of the $[Be]^+$ (measured at 4 K, solid circles) and V_{OH} centres (measured at 80 K, open triangles). Solid curves are guides for the eye.

into two groups when the magnetic field is along <100> type axis (Fig. 9). The perpendicular group (the left one in the figure) consists of four lines while in the parallel group they build up one single absorption band. This obviously shows a hyperfine interaction between spin S =1/2 and nuclear spin I = 3/2. The crystals used in the experiment have quite a high concentration of Be^{2+} ions with spin I_{Be} = 3/2 which manifests itself as the nucleus in the discovered centre. The initial experimental estimates on the centre g-factor showed a positive g-factor shift from the free electron one which defines the spin S = 1/2 as a hole. The centre was named $[Be]^+$ with the following structure: $Be^{2+} – O^-$.

The roadmap of the centre, calculated in the {100} plane (Fig. 10) shows a tetragonal symmetry with a slight orthorhombic distortion. The fitting of the experimental data was performed using EPRNMR software by Weil et al., and the results are tabulated in Tab. 4. The Euler angles here describe the defect axes with respect to the principal axes of the crystal, namely, the defect X axis coincides with the <110> axis, Y and Z axes lie in a {100} plane and are deflected by ~2.5° from, <001> and $< 1\bar{1}0 >$ directions, respectively.

Table 4. EPR spectrum parameters for $[Be]^+$ centre. Euler angles α, β, γ show the defect axes direction with respect to principal <100> axis of MgO. First 3 columns show the diagonal components of the tensor

	x	*y*	*z*	*α*	*β*	*γ*	*a, MHz*	*b, MHz*
g	2.0465	2.0447	2.0045	-2.86	2.42	45.29	1.01	-0.54
A	1.64	1.49	-0.08					

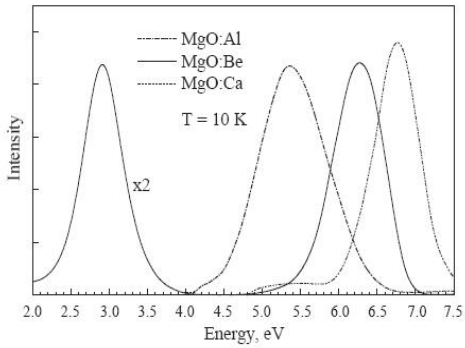

Figure 12. Cathodoluminescence of MgO crystals doped with Al, Be and Ca at 10 K

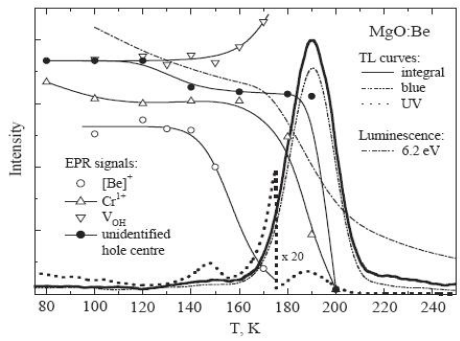

Figure 13. Thermoluminescence of MgO:Be crystals recorded at 2.9 eV ("blue") and 6.2 eV ("UV"), thermal quenching of the 6.2 eV luminescence

The thermal dependence of the $[Be]^+$ EPR signal strength was measured (Fig. 11). According to our results, at temperatures T > 40 K, the EPR signal can no longer be observed. It is worth mentioning that there was no motion averaging of the EPR spectrum at all in the observable temperature range. The thermal stability of this centre was investigated using isochronal annealing technique (Fig. 11), i.e. the crystal was heated to the temperature corresponding to the experimental point and then recooled to a temperature of the best observed EPR spectrum (4 K in this particular case). Also these measurements show T ≈ 150 K being a temperature of thermal destruction of the centre, later investigations [VI, VII] showed a systematic error in the experimental equipment. The corrected temperature of the thermal destruction of $[Be]^+$ centre is T = 195 K. At the same time, at this temperature, the number of V_{OH} centres is rapidly increasing. This is probably due to the existence of V_{OH}^- centres which act as a good trap for the holes released from $[Be]^+$ centre, hence creating stable (in the considered temperature range) V_{OH} centres:

$$Be^{2+}O^- \rightarrow Be^{2+}O^{2-} + e^+;\ V_{OH}^- + e^+ \rightarrow V_{OH}$$

We have measured [IV] the cathodoluminescence (CL) of $[Be]^+$ centre at 10 K (Fig. 12). The luminescence peaks arise from a recombination of electrons with the holes localized in various defects centres: the V-centres in MgO:Al (5.3 eV), the $[Be]^+$ centre in MgO:Be (6.2 eV) and presumably $[Ca]^+$ centre in MgO:Ca (6.8 eV). The thermoluminescence (TL) spectrum was recorded in the whole spectral range (integral spectrum) and in the two main luminescence peaks: 2.9 eV and 6.2 eV (Fig. 13). The 6.2 eV peak in TL spectrum appears only in Be-doped MgO crystals which is consistent with the CL peak. In addition to that,

the TL spectrum shows UV peak at 147 K where the EPR signal of $[Be]^{+}$ starts decreasing, which can be caused by a recombination of a conduction electron with the hole localized next to a beryllium ion. At the same time, the TL peak at 147 K can be associated with the thermal destruction of Be^{1+} centres, which can cause the decline in the luminescence intensity visible in that region. The difficulties in interpretation here arise from the fact that there are numerous centres decaying in this temperature region (150 – 200 K).

3.4.1.2. Temperature dependence of the EPR spectrum

To find the temperature dependence of the $[Be]^{+}$ EPR spectrum we have measured the spectra for the temperatures T = 5.2 K, 10 K, 15 K, 24.4 K

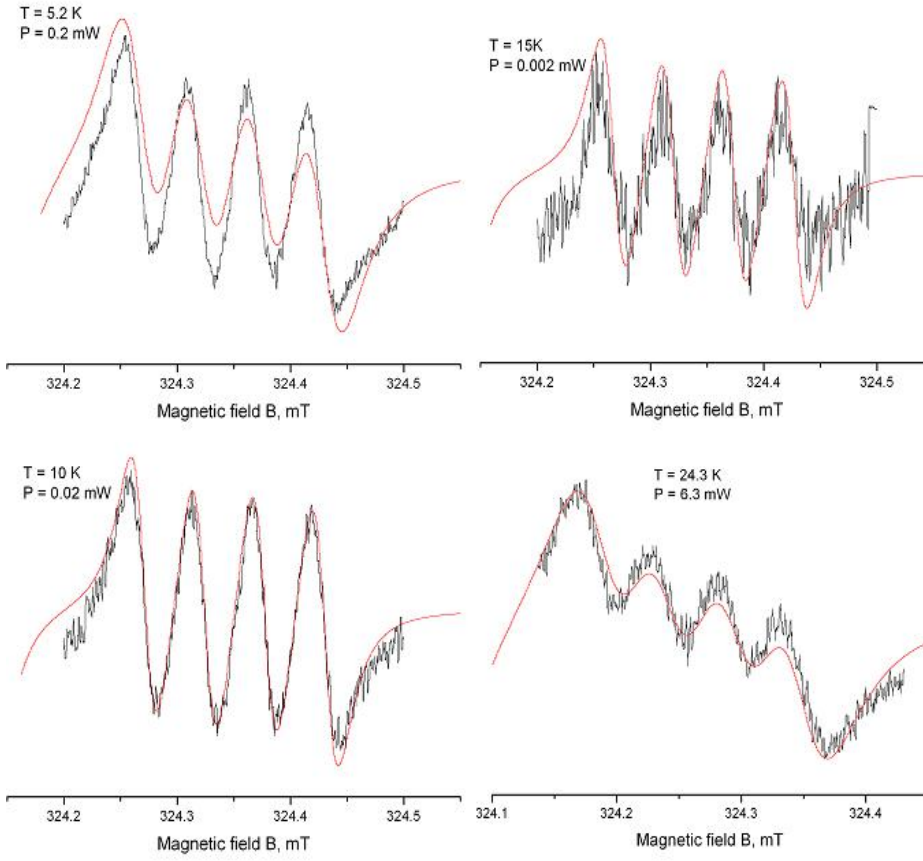

Figure 14. Comparison of theoretical (red lines) and experimental (black lines) EPR spectra for different microwave powers and temperatures. Spectra are simulated using VirtualEPR Spectrometer

with microwave powers P = 2 μW, 6.3 μW, 20 μW, 63 μW, 200 μW, 630 μW, 2 mW, 6.3 mW and 20 mW [V]. The experimental data were fitted with a lorentzian lineshape to measure the exact linewidth of the EPR absorption band. Upon fitting, only the perpendicular group of four lines was taken into account.

The spin-spin relaxation time was found at very weak microwave powers: $\tau_2 = 2.8 \cdot 10^{-7}$ s. The dependence of the spin-lattice relaxation time on temperature was found based on the Kronig-van Fleck mechanism parameters. Fitting of the experimental data at microwave powers when EPR signal saturates, led to the following result: a = 420, $b = 2 \cdot 10^{-5}$ with n =7, c = 0. A comparison of the experimental and theoretical spectra for different values of microwave power and temperature reveals quite a good agreement (Fig. 14).

3.4.1.3. Data analysis

The big difference of $[Be]^+$ centre compared to the trapped-hole centres in MgO described above is that it does not have a tetragonal symmetry. There is a reduction in symmetry due to an excess positive charge of the defect and small ionic radius of Be^{2+} $r_{Be} = 0.45$ Å $= 0.6 r_{Mg}$. The Coulomb interaction between the Be^{2+}, O^- ion and the neighbouring ions should obviously attract the beryllium ion to neighbouring ions outwards the O^- ion, along the <100> principal axis of MgO. At some point, an overlap between Be^{2+} and the adjacent along the <100> axis O^{2-} cores occurs, which acts as a repulsion force. Due to the small ionic radius of Be^{2+}, it can relax away from the <100> axis in {001} plane, localizing somewhere between to oxygen ions. Neglecting the deflection of Y and Z defect axes from the {100} plane and taking into account that $r_{Mg} + r_O \approx a_0$ in the first approximation, the relaxation of Be^{2+} ion can be represented by means of simple geometry (Fig. 15). Solving the triangle equation and applying some transformations leads to the following formula for the distance between O^- and Be^{2+} ions:

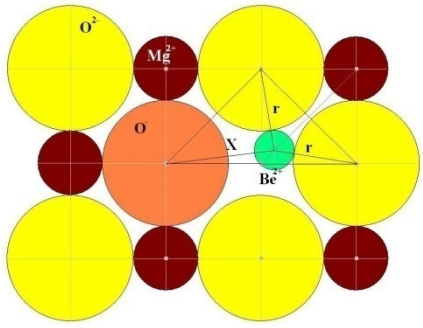

Figure 15. Geometric representation of $[Be]^+$ centre.

$$X^2 = \frac{a_0^2 + 2r^2 - a_0\sqrt{8r^2 - a_0^2}}{2},$$

where a_0 is a lattice constant, r – contact radius between O^{2-} and Be^{2+} ions $r = r_{Be} + r_O$. In this case, the distance between ions is X = 2.4 Å

≈ $0.6a_0$. It is worth noting, that due to the symmetry the shift will be in <110> direction which is in a good agreement with defect axis description by the Euler angles.

The distance between the hole and Be^{2+} ion can also be calculated using hyperfine interaction parameters (Tab. 4). Based on formula (5a), the overlap between the hole and Be^{2+} wave function can be calculated by comparing the experimental isotropic hyperfine constant *a* with theoretical for Be 2S orbital A_{0Be} = –381 MHz [32]: $a/A_{0Be} = 0$. This result allows application of the point-dipole approximation for describing the interaction between the hole and beryllium ion. From formula (5b) the distance *l* between the latter can be calculated, which gives *l* = 2.944 Å ≈ $0.7a_0$. This is in a quite good agreement with the geometrical description of the centre, namely there is an outwards relaxation between Be^{2+} and O^- ions. It is obvious that ions surrounding the centre should also slightly relax away from their central positions. All such relaxations lead to an increase in the potential well depth which acts as a trap for the hole. Anyway, the potential well depth is quite small which manifests itself in a low temperature of thermal destruction T = 195 K.

3.4.2. $V_{OH\text{-}Be}$ centre

3.4.2.1. Experimental results

When MgO:Be single crystals are subjected to x-irradiation at room temperature (RT) a new paramagnetic centre is formed [I, III]. The paramagnetic resonance spectrum of this centre can be observed in the range of 40 K to the room temperature (Fig. 16). Below 40 K the saturation of the EPR signal of the centre prevents its detection. At an arbitrary angle between the static magnetic field **B** and MgO <100> type axis in a {001} plane, a three separate groups of lines can be observed. There is an obvious separation of these groups into two smaller groups of lines. When the angle between the static magnetic field and <100> principal axis is 0° and 45°, two groups coincide, leaving only two bigger groups of lines.

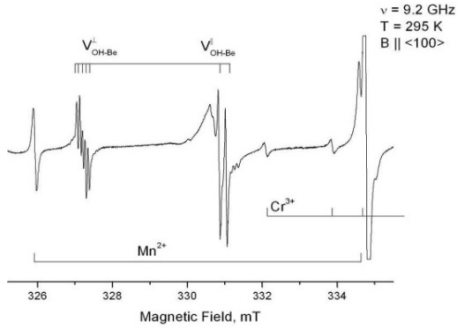

Figure 16. Experimental EPR spectrum of $V_{OH\text{-}Be}$ centre measured at RT with a static magnetic field parallel to the MgO <100> type axis.

Table 5. Parameters of $V_{OH\text{-}Be}$ centre. SHF interaction parameters are separated for H^+ and Be^{2+} ions.

$V_{OH\text{-}Be}$	$g_\perp$	$g_{\|\|}$	$A_\perp$, *MHz*	$A_{\|\|}$, *MHz*	*a, MHz*	*b, MHz*
Be^{2+}	2,0250	2,0023	2,085	0	1,385	-0,692
H^+			-2,085	5,212	0,366	2,423

The roadmap (Fig. 17) shows the tetragonal symmetry of this centre. Such spectrum can be achieved by interaction between spin S = 1/2 with 2 nuclear spins I = 3/2 and I = 1/2. Taking into account that MgO:Be crystals were cloudy, the only possible nuclei with such spins are beryllium and hydrogen. This centre was named $V_{OH\text{-}Be}$ with the following structure: $Be^{2+} – O^- – v_c – OH^-$. At this point it is noticeable as if structure of $V_{OH\text{-}Be}$ centre is a summation of $[Be]^+$ and V_{OH} centres . Measured parameters of $V_{OH\text{-}Be}$ centre were fitted using EPRNMR software (Tab. 5).

We have measured the absorption spectrum of x-irradiated MgO:Be single crystals and compared it to the one of MgO:OH (Fig. 18). An increase in absorption coefficient can be observed. The difference between the absorption spectra for these two crystals shows an approximate position of the $V_{OH\text{-}Be}$ centre absorption band at ~3.2 eV. The temperature of centre destruction by thermal release of the hole measured by TL is 400 K which is between thermal destruction temperatures of V_{OH} and V^- centres.

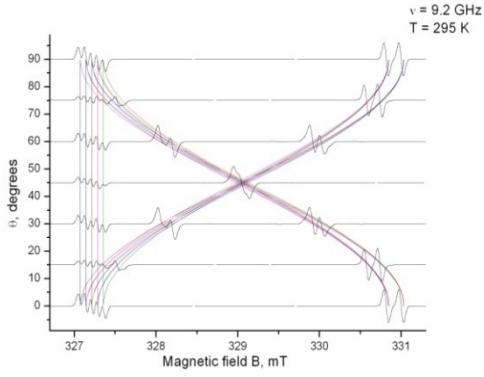

Figure 17. Roadmap of $V_{OH\text{-}Be}$ centre calculated with the EPRNMR software. The spectra are simulated using the VirtualEPR Spectrometer. Angle θ is between the magnetic field **B** and <100> type axis.

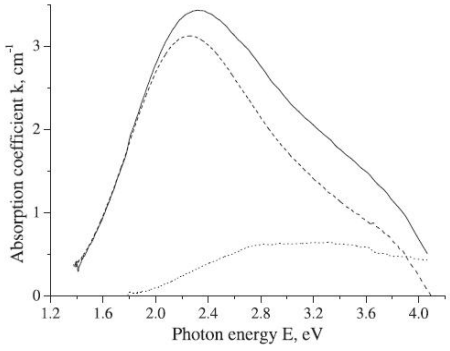

Figure 18. The additional optical absorption of MgO:Be (solid curve) and MgO:OH crystals (dashed curve) induced by x-irradiation (295 K, 50 kV, 100 Gy), measured at RT. The dotted curve depicts the difference of these two absorption curves.

3.4.2.2. Temperature dependence of the EPR spectrum

The temperature dependence of the $V_{OH\text{-}Be}$ EPR spectrum was measured. for temperatures T = 90, 110, 120, 130, 150, 170, 200, 250, 195 .2 K, 10 K, 15 K, 24.4 K with microwave powers P = 2 μW, 6.3 μW, 20 μW, 63 μW, 200 μW, 630 μW, 2 mW, 6.3 mW, 20 mW and 160 mW [V]. The experimental data were fitted using the lorentzian lineshape (homogeneous broadening) to measure the exact linewidth of the EPR. Upon fitting only the perpendicular group of five lines was taken into account.

The spin-spin relaxation time was found at very weak microwave powers: $\tau_2 = 2.8 \cdot 10^{-7}$ s. The dependence of spin-lattice relaxation time on temperature was found based on the Kronig-van Fleck mechanism parameters. The fitting of experimental data at microwave powers when the EPR signal saturates, led to the following results: a = 420, b= $2 \cdot 10^{-5}$ with n =7, c = 0 which are in a good agreement with the experiment.

3.4.2.3. Data analysis

It was already stated that the $V_{OH\text{-}Be}$ centre can be represented as a summation of $[Be]^+$ and V_{OH} by structure. It was shown above, that in $[Be]^+$ centre a hole is trapped due to the electric dipole created by the relaxation of a Be^{2+} ion from the central position of a cation vacancy. The same mechanism in $V_{OH\text{-}Be}$ centre implies an addition to the local potential well depth as compared to the V_{OH} centre, giving the former more stability: the temperature of the thermal destruction of the $V_{OH\text{-}Be}$ centre is T = 400 K which is much higher than that for V_{OH} centre (T = 335 K). This statement can be proved using hyperfine interaction parameters a_{Be} and b_{Be} of the $V_{OH\text{-}Be}$ centre (Tab. 5). Again, due to a small ratio between the experimental and theoretical isotropic hyperfine parameters, the point-dipole approximation can be applied to calculate the distance between the O^- to Be^{2+} ions giving l_{Be} = 2.739 Å ≈ $0.65a_0$, which is quite close to the one of $[Be]^+$ centre.

The validity of equality $V_{OH\text{-}Be} = [Be]^+ + V_{OH}$ can also be shown using the perpendicular g-factor shift of these centres. From formula (4a) the separation between $p_{x,y}$ and p_z states of O^- ion can be estimated using oxygen spin-orbital coupling parameter λ_O = 0.0167 eV. The following values for every centre can be obtained: $\delta_{OH\text{-}Be}$ = 1.47 eV, δ_{OH} = 0.89 eV, $\delta_{[Be]+}$ = 0.77 eV. A comparison of values for $\delta_{OH\text{-}Be}$ and $\delta_{OH} + \delta_{[Be]+}$ = 1.66 eV shows a reasonable agreement between them.

An open question here is the relaxation of the surrounding ions. Assuming that there is no such relaxation and taking into account the tetragonal symmetry of the defect, the outward relaxation of the Be^{2+} ion should be along the <100> type axis with a maximum possible distance to O^- ion $X = a_0 - r_O - r_{Be} = 2.362$ Å as it follows from the geometrical picture (Fig 15). Considering the distance from H^+ to O^-, calculated using the hydrogen anisotropic hyperfine constant (point-dipole approximation can be applied here as well, due to $A_{0H} = 1420$ MHz [2]) $l_H = 3.398$ Å $\approx 0.8a_0$, the relaxation of O^- ion from its central position away from Be^{2+} ion is expected Such relaxation can be approximated using $\Delta X = 1.5a_0 - (l_{Be} + l_H) \approx 0.2$ Å. Taking into account the experimental data errors, one can state that there is no or very small relaxation of the ions surrounding the $V_{OH\text{-}Be}$ centre. In its turn, the big relaxation of the hydrogen ion from the centre of cation vacancy $l_H = 0.8a_0$ means there is a molecular bonding with oxygen O^{2-} building the OH^- group which proves the defect structure.

3.5. Comparison

A summary of different hole centres in pure and doped MgO single crystals is given in Table 6. The centres are ordered by the g-factor shift showing, different contributions to the hole trapping mechanism.

For the monovalent $[Na]^0$ and $[Li]^0$ centres, the Columbic interaction causes the hole to localize on the oxygen ion due to an excess positive charge as compared to Mg^{2+}. In the case of $[Li]^0$ centre, there exists an electric dipole created due to an outward relaxation of the Li^+ ion from the central vacancy position ($l \approx 0.6a_0$) as in the case of $[Be]^+$ centre which creates an electric dipole that deepens the potential well in addition to the Columbic interaction. Such relaxation is possible since the lithium ionic radius is smaller than that for magnesium ion: $r_{Li} = 0.76$ Å [14] and is consistent with the above-described geometrical approximation.

This is not the case for the $[Na]^0$ centre. In Tab. 6 the distance between Na^+ and the hole localized on O^- ions ($l \approx 0.45a_0$) shows an inward relaxation of the former, which obviously manifests an overlap between the sodium and oxygen cores. This shows some inconsistency in the point-dipole approximation used for calculating the distances: the ratio between the isotropic hyperfine parameter with theoretical value for Na 3S orbital $A_{0Na} = 927.1$ MHz [32] is $a/A_{0Na} = 0.007$, while there is an obvious overlap between the cores. In [4] the calculation based on the electric field gradients extracted from the constant of quadrupole

Table 6. Summary of the hole centres discovered so far in pure and doped MgO single crystals

		$\Delta g_{\perp}$	a, MHz	b, MHz	l, Å	p, %	T, K	δ, eV	E_{absorp}, eV	E_{lumin}, eV
$V_{OH\text{-}Be}$	Be	0,0227	1,385	-0,692	2,739	0,0	400	1,47	3,20	
	H		0,366	2,423	3,398					
V_{Al}		0,0363	0,011	0,083	6,495	2,8	375	0,92	2,33	5,3
V^{-}		0,0363					420	0,92	2,33	5,3
V_{OH}		0,0375	0,101	2,371	3,421	2,7	335	0,89	2,21	
V^{0}		0,0385					345	0,90	2,36	
$[Be]^{+}$		0,0433	1,009	-0,544	2,944	5,1	195	0,77		6,3
$[Li]^{0}$		0,0522	-4,538	2,313	2,590	5,0	230	0,64	1,83	5,6
$[Na]^{0}$		0,0702	-6,387	4,706	1,893	4,8	190	0,48	1,34	
$[Ca]^{+}$							48			6,8

interaction with crystal field produced a similar relaxation distance as for the point-dipole approximation that is probably a coincidence. One thing should be noted here anyway: one should use hyperfine interaction parameters with great care for the cases when there is a possible overlap of the ionic cores in terms of simple geometry.

The above-described similarities and differences in the structure of $[Li]^{0}$ and $[Na]^{0}$ centres have several consequences in their physical properties. Firstly, the temperature of centre destruction by the thermal release of the hole is 40 K more for $[Li]^{0}$ centre, while for $[Na]^{0}$ centre this temperature is almost the same as for $[Be]^{+}$ centre where there is a net positive charge. Secondly, the first excited hole energy level is much lower for $[Na]^{0}$ centre. Thirdly, one can note that the ratio between the interpolaron (absorption) and intrapolaron (O^{-} $p_z \rightarrow p_{x,y}$) transitions for these centres is almost the same:

$$E_{abs}^{[Na]^0}/\delta_{[Na]^0} = 2.79,$$

$$E_{abs}^{[Li]^0}/\delta_{[Li]^0} = 2.83.$$

This is consistent with the probability of spontaneous transfer of the hole from the axial O^{-} ion to equatorial ones, i.e. interpolaron transitions, calculated for both centre using $p = \Delta g_{||}/\Delta g_{\perp}$. These values are presented in Table 6.

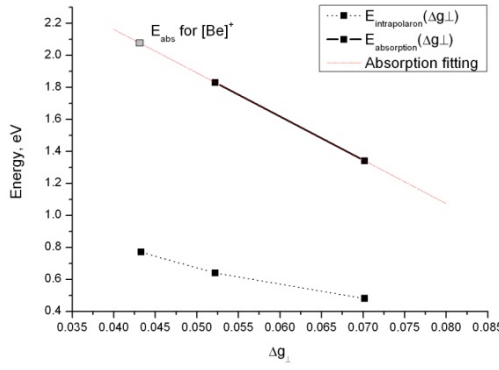

Figure 19. Intra- and interpolaron transition energy dependence from g-factor shift for $[Li]^{0}$, $[Na]^{0}$ and $[Be]^{+}$ centre. Interpolation shows the approximate absorption energy for the latter.

One can notice that there is almost linear dependency between the energy of the intra-

polaron transition and g-factor shift for the $[Be]^+$, $[Li]^0$ and $[Na]^0$ centres (Fig. 19). Subsequently, the absorption energy for the $[Be]^+$ centre can be estimated by the linear interpolation of the dependence of the absorption energy of the $[Li]^0$ and $[Na]^0$ centres from the g-factor shift, giving $E_{abs}^{[Be]^+} \approx 2.2\ eV$ (Fig. 19). The overlap of this estimate with the position of the V_{OH} centre absorption band could be a reason why there is no experimental identification of $[Be]^+$ absorption band yet.

3.6. Self-trapping of a hole

The problem of the hole self-trapping in MgO single crystals has long been under consideration. The only work that supported the existence of self-trapped excitons was carried out in Latvian State University by Rachko et al [33]. At thermal quenching of the luminescence they discovered an intensity increase of 6.9 eV band in both undoped MgO single crystals and those doped with different impurities. Anyway, there have been no more papers from the Latvian team on the same topic. Also, it turned out that MgO crystals used in the experiment were quite "dirty" contrary to what they stated. At the Institute of Physics, Tartu, the only experimental evidence of that peak was found in Ca-doped MgO crystals which is assigned presumably to $[Ca]^+$ centre (Ca^{2+} substituting Mg^{2+} next to the hole trapped on the oxygen ion). Moreover, in theoretical calculations, Shluger et al. showed that there cannot occur any self-trapping of holes in a bulk MgO crystal, while this is possible at low-coordinated sites (corners, kinks etc.) at MgO (100) surface [34]. Such conclusion is consistent with the experimental results by Elango et al. [35] who showed a high hole mobility in the bulk MgO.

A similar conclusion is drawn from the experimental data for the described trapped-hole centres. Apparently, hole trapping in MgO single crystals can happen only if there exists an initial distortion or irregularity in the crystal. For example, $[Li]^0$ and $[Na]^0$ centres are formed after crystal irradiation from $[Li]^+$ and $[Na]^+$ centres, respectively, which are present in the "as grown" crystals. V-type centres are formed from the V_{OH}^- centre existing in the "as grown" crystals as well. In general, one can follow the line of trapped-hole centres by decrease of different contributions to the defect shown by the g-factor shift: $[Be]^+$ – $[Na]^0$ – $[Li]^0$ – V_{OH} – V_{Al} – V^0 – V^- – $V_{OH\text{-}Be}$, i.e. electric dipole, Columbic interaction with an electric dipole, cation vacancy and, finally, a cation vacancy with an electric dipole.

A “lonely” member of this group is the $[Be]^+$ centre which does not have any obvious precursor for the hole trap. Due to the small ionic radius, the Be^{2+} is hopping in the cation vacancy site polarizing the surrounding oxygen ions. When MgO:Be crystal is then subjected to irradiation, such polarizations act as shallow traps for the holes. At some point, when a hole localizes at the O^{2-} neighbouring the Be^{2+}, the latter relaxes away from the former, hence, the potential well is deepened so that its depth is sufficient for localizing the hole. As Be is isovalent with Mg, there are no other forces that localize the hole.

In view of this, it could have been very instructive to investigate hole trapping in MgO:Ca crystals. Ca is also isovalent with Mg, but its ionic radius r_{Ca} = 1.00 Å is comparable with the sodium ionic radius and is much bigger than that of magnesium. Such a big ion will produce local distortions at the cation vacancy site thus allowing a hole to be trapped on the neighbouring O^{2-}, forming $[Ca]^+$ centre. In [36], the peak of thermal destruction of possibly $[Ca]^+$ centre was identified at 48 K and 6.8 eV luminescence peak was assigned. Unfortunately, the experimental technique in the magnetic resonance laboratory does not allow any EPR spectrum observations for this centre because it must be irradiated and kept before the measurements at T < 30 K which is impossible to do right now. Theoretically, this centre can be observed at T < 4 K in the g-factor region of 2.05 – 2.10 [II]. This is a topic for future investigations given the modern experimental equipment.

4. INTERSTITIAL CENTRES

Highly pure MgO crystals are extremely resistant against γ- and X-rays. At the same time the irradiation of MgO by fast protons, neutrons or ions causes an efficient creation of F^+ and F centres (one or two electrons in the field of an anion vacancy, respectively – $v_a e$, $v_a ee$). For years such radiation damage has been related to the creation of Frenkel defects in an anion sublattice, i.e. interstitial centres, due to the knock-out (impact) mechanism, universal for solids, that is connected with elastic collisions of high-energy particles with the atoms/ions of a crystal. Such oxygen interstitial centres are the least investigated type of Frenkel defects in MgO as well as in all wide-gap metal oxides while they play a crucial role in determining the response of MgO single crystals to high-energy particles irradiation.

4.1. Formation of the H centres with a knock-out mechanism

The existence of interstitial centres was first reported by Halliburton and Kappers in 1978 [37], who measured the EPR spectrum of the oxygen interstitial centres in neutron-irradiated MgO single crystals. Since then almost no research was carried out on the topic until 2000 when Kärner et al. reported new experimental data on the TL of the oxygen interstitial centres in pure and doped MgO crystals [38, 39, 40].

4.1.1. EPR evidences of the H centres

When MgO:Al single crystals are subjected to neutron irradiation with an average energy of 2 MeV and fluence of about $10^{14} – 10^{17}$ neutron/cm^2 new paramagnetic centres of a similar structure (Fig. 20) are formed [39]. Both centres have a similar g-factor shifted slightly from each other: g_{Ix} = 2.0059, g_{Iy} = 2.0011, g_{Iz} = 2.0767, θ = 30.46° and g_{IIx} = 2.0061, g_{IIy} = 2.0011, g_{IIz} = 2.0761, θ = 31.24°, where θ is the angle between the defect main axis and MgO <100> principal axis. These centres were identified as H centres, namely a trapped-hole interstitial oxygen molecule O_2^- next to a cation vacancy.

First of all, the g-factor shows a positive deviation from the free-electron one, which is a sign of a trapped-hole centre. But unlike V-type centres, the ordering of g-factor components is the opposite, with the parallel term having the highest value. Känzig and Cohen [41] initially studied such molecules in alkali halides and showed that the O_2^- molecule exhibits such behaviour. Secondly, the slight difference between

g-factors and defect axis angle for the observed spectrum (Fig. 20) is most likely due to small perturbations by the neighbour ions. As a matter of fact, in the similar experiment performed by Halliburton and Kappers, they observed three different EPR signals in the same spectrum with similar deviations in the g-factor for every signal, with one of them showing a small SHF splitting. Hence, the oxygen interstitials are stabilized by the same entity present in the MgO crystals, namely the cation vacancy. In general, along with simple H centres, there exists a family of H_M centres where M denotes the neighbouring cation or anion impurity. Kärner et al. [39] proved these statements, when another MgO:Al crystal with a twice higher concentration of Al^{3+} dopant was subjected to neutron-irradiation. Only the signal from H_I centre was observed in the EPR spectrum with a 10 times higher intensity.

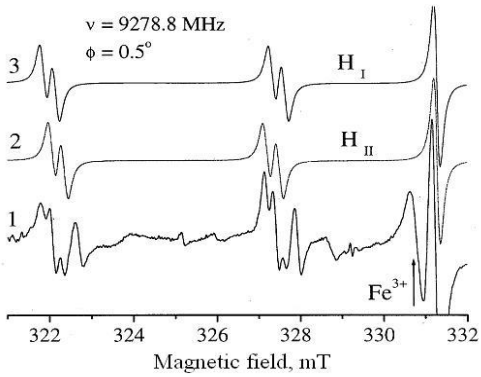

Figure 20. EPR spectra of the neutron-irradiated MgO single crystal. 1-experimental spectrum, 2 and 3-computer simulated spectra for H_I and H_{II} centres, respectively. ϕ is the angle between the magnetic field and <110> crystal direction

Although holes can self-trap in halide lattices at a low temperature to form X_2^- molecules, there is no evidence of an analogous behaviour in the simple oxides. It is then considered quite unlikely that two adjacent lattice oxygen ions could join together to form a O_2^- molecule, especially taking account of an almost tight binding of the ions in the MgO lattice. The only viable alternative is that oxygen interstitials are created during neutron irradiation via the knock-on mechanism. They migrate in the lattice till they are trapped by a cation vacancy or some other impurity. Finally, interstitial combines with the adjacent lattice oxygen ion forming a O_2^- molecule (Fig. 21):

$$O_i^0 + O^- + v_c \rightarrow O_2^- v_c$$

It is worth mentioning, that no interstitials are observed in MgO single crystals after X-ray of gamma ray irradiation. This is consistent with the fact that the energy of creating a Frenkel defect in MgO calculated in adiabatic approximation E_{FD} = 15.2 eV [31] is more than the band gap E_g = 7.83 eV, which means that an electron-hole recombination or decay of an anion excitons ($E_{exciton}$ = 7.7 eV) is not sufficient to create an interstitial O_2^- centre.

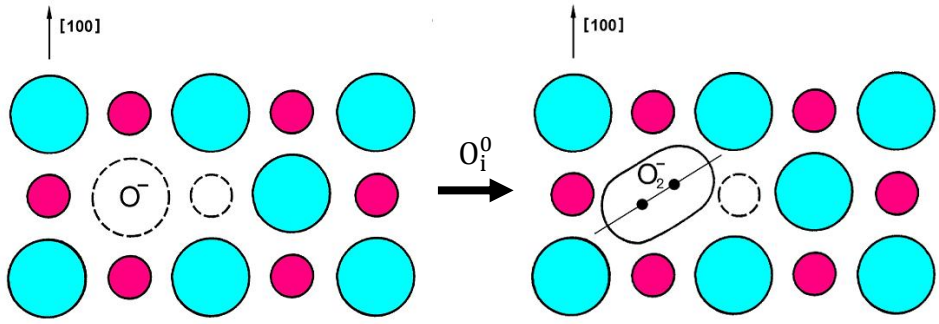

Figure 21. Stabilization of H centre next to a trapped-hole centre in a MgO crystal

4.1.2. Manifestation of Frenkel defects in thermoluminescence

The irradiation of MgO by fast neutrons at 300 K leads to the creation of F^+ centres (the maxima of absorption and emission bands are at 4.95 and 3.15 eV, respectively) and a smaller amount of F centres (the absorption peak at 5.03 eV and the emission one at 2.4 eV) [42]. The same optical characteristics have been detected in our samples of MgO (pure crystals, MgO:Al, MgO:Be) previously irradiated by ~2 MeV neutrons with a fluence of 10^{14}–10^{17} n/cm^2 at room temperature. Significant changes in the thermoluminescence spectrum of the crystals were observed (Fig. 22): the decrease of the intensity of low temperature peaks and the emergence of high temperature TL peak at ~700 K [40].

Before every measurement, the crystals were subjected to a control X-irradiation. During the first measurement, the crystals were heated up to 773 K when H centres were destroyed which is observed upon the

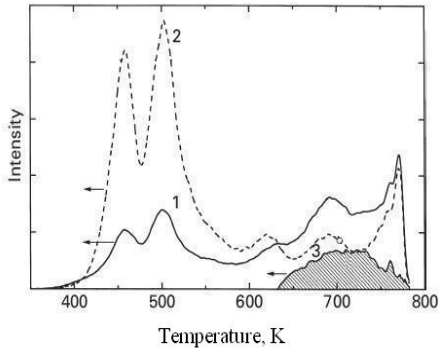

Figure 22. The high temperature TL spectra of the neutron irradiate MgO. 1 – the first measurement, 2 – the second measurement, 3 – the difference between the light output at 700 K

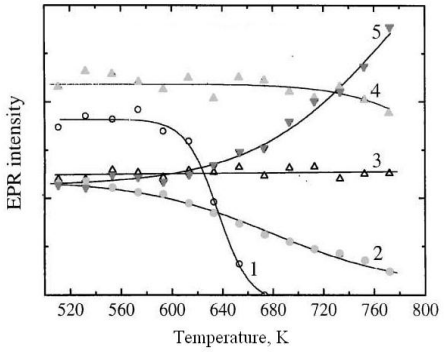

Figure 23. The isochronal annealing of the EPR signal intensity of the neutron-irradiated MgO:Al crystal measured at 100 K. 1 – H, 2 – F^+, 3 – Mn^{2+}, 4 – Fe^{3+}, 5 – Cr^{3+} centres.

isochronal annealing of the EPR signal intensity measured at 100 K (Fig. 23). At the same time, the intensity of the Cr^{3+} centre is quickly increasing. The second measurement showed an increase in the low-temperature region T < 550 K, which according to Luthra et al. [43], is an evidence of thermal destruction of trapped-hole centres. The difference in the light output (Fig. 22, 3) showed a linear dependency of the neutron fluence in the range of the experiment (10^{14} – 10^{17} neutron/cm^2). This property of H centres can be used in the selective dosimetry of fast neutrons [40].

The behaviour of TL peaks during two measurements combined with the isochronal annealing of EPR signals of different centres suggests the following thermal destruction of an H centre:

$$(O_2^-)v_c \rightarrow O_i^0 + v_c + h$$

The frequency factor measured for the TL curve of an H centre stays at the level 10^{12} – 10^{14} cm^{-1} in the temperature range of 450 – 630 K which means normal hole-electron processes. The factor then rapidly decreases by almost four orders in the range of 650 – 700 K, which may be related to the hopping diffusion of a neutral oxygen atom as it was interpreted for the V_K centre in NaCl:Ag [44]. During such diffusion, the neutral oxygen will recombine with an F^+ centre (electron localized on an anion vacancy):

$$O_i^0 + F^+ \rightarrow O^{2-} + h$$

The released holes can be captured by Cr^{2+} impurity forming Cr^{3+} centres:

$$Cr^{2+} + h \rightarrow Cr^{3+*} \rightarrow Cr^{3+} + h\nu,$$

with luminescence in the red spectral region. This formation mechanism is fully supported by the experimental data: interstitial destruction is followed by the destruction of F^+ centres (Fig. 23), although the rate of the intensity decrease is quite different. At the same time, the released holes drastically increase the number of Cr^{3+} centres.

4.2. Non-impact mechanism of interstitial formation

The above-described neutron irradiation of MgO crystals is a commonly accepted way of formation of stable Frenkel defects: anion vacancy with an interstitial oxygen. The stabilization of the former leads to F and F^+ centres by electron capture, while the neutral interstitial is localized next to the trapped-hole centre forming the H centre. In the present study, the non-impact creation and stabilization of oxygen interstitials under conditions of a high density of electronic excitations formed in the tracks of swift heavy ions (SHI) is considered on the example of undoped and

Be-doped MgO single crystals. Novel radiation effects are found at high excitation densities.

4.2.1. Experimental results

In this work, a low-temperature investigation of the cathodoluminescence of the three pure MgO crystals has been performed in the effort to test the non-impact mechanism of the Frenkel defects creation [VI, VII]. One crystal was thermochemically coloured (i.e. containing a certain amount of F centres) and two other highly pure crystals were previously irradiated by fast neutrons (~2 MeV, fluence $10^{14} - 10^{17}$ n/cm^2) or swift uranium ions (2.25 GeV, fluence 2×10^{11} ions/ cm^2) at 300 K. The probing of the samples was performed by a weak beam of 5 – 15 keV electrons at 6 K. Such electrons are not able to create additional radiation defects but can excite the recombination luminescence at the interaction of electrons and holes (formed at an electron-irradiation) with the already existing defects. The penetration depth of such electrons calculated by the Casino software using the Monte Carlo method produced the peak concentration at 13.5 and 920 nm from the surface with the maximum depth of 200 and 1200 nm, for 5 and 15 keV electrons, respectively. The CL spectra for the three cases are presented in Fig. 24.

4.2.2. Probing of defects in pure MgO crystals by slow electrons

Probing of the thermochemically coloured MgO crystals by slow 5 keV electrons does not produce any significant difference in the intensities of F and F^+ centres (Fig. 24, a), while probing of the neutron irradiated crystals shows a rapid growth of the F centre emission peaked at 2.4 eV (Fig. 24, b, the experimental shape is slightly distorted by the reabsorption on other defects). This result strongly supports a commonly accepted opinion that neutrons mainly create the F^+ centres. These F^+

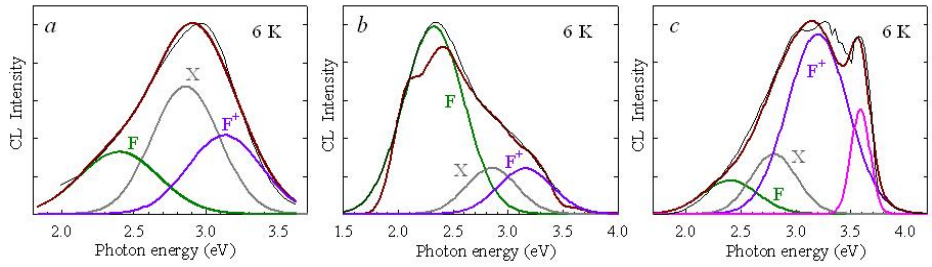

Figure 24. Cathodoluminescence spectra for a) thermochemically colored, b) neutron irradiated at 300 K (~ 2 MeV), and c) swift uranium ions irradiated at 300 K (~ 2 GeV) MgO crystals. CL is measured at 6 K. The F and F+ centres emission bands are shown. The X emission band is associated with a crystal stress.

centres serve as radiative traps for conduction electrons, formed at an additional electron irradiation, and the F-emission is detected in the cathodoluminescence spectrum according to the following reaction: $F^+ + e \rightarrow F^* \rightarrow F + hv\,(2.4\,eV)$. It should be noted that the neutron irradiated sample was uniformly coloured in the thickness of 1 mm, while the maximum penetration depth of the probing 5 keV electrons is much smaller (200 nm).

The CL spectrum of the uranium irradiated pure MgO crystals shows an even more different behaviour (Fig. 24, c). The emission of the F^+ centre here dominates over the emission of the F centre by almost an order of magnitude. This can be explained by a high concentration of single anion vacancies in the ion tracks due to their efficient creation by swift heavy ions (SHI) irradiation which as radiative traps for the probing electrons forming F^+ centres: $v_a + e \rightarrow F^{+*} \rightarrow F^+ + hv(3.15\,eV)$. The radiative trapping of the second electron causes the formation of an F centre as in the case of a neutron irradiated crystal, while the amount of such centres is smaller than that of F^+ centres.

Taking into account the penetration depth of the uranium ions (~ 70 μm) and the fact that 99.9 % of the energy of 2 GeV uranium ions is spent on the electron energy losses followed by the collision with the lattice ions at the end of the track, it is obvious that the formation of anion vacancies and the complementary oxygen interstitials is due to the formation of various electronic excitations in the uranium ion tracks. As a result, a large amount of non-relaxed (hot) holes and conduction electrons are formed in the ion tracks. The interstitial centres are partly created because of their hot recombination. A detailed study of other possible non-impact mechanisms of radiation damage still lies ahead.

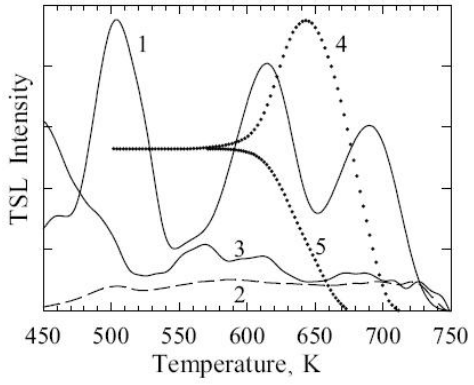

Figure 25. Integral TL measured for MgO irradiated by ^{238}U ions (1), fast neutrons (2) and α particles (3) at 300 K. The annealing of the EPR signal of H (4) and H_X centres (5) in neutron-irradiated MgO.

The existence of the interstitial H centres complementary to F^+ centres is confirmed by the TL spectrum of the swift uranium ions irradiated MgO crystals (Fig. 25): the characteristic peak of the thermal destruction of H_X centre at 620 K (H centre perturbed by an unidentified impurity) and H

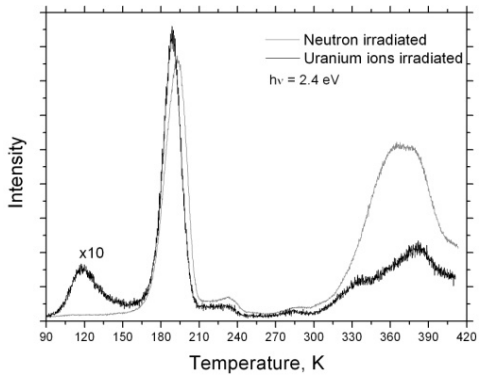

Figure 26. The TL spectra of MgO:Be crystal irradiated by neutron and swift uranium ions measured at 2.4 eV.

centre at 690 K. The comparison of this spectrum with the TL of neutron irradiated MgO crystal shows a significant difference in the amount of stable H centres in the MgO crystals. In addition, the TL spectrum comparison of the neutron and swift uranium ion irradiated Be-doped MgO crystals (Fig. 26) shows a slight displacement of the TL peak to the lower temperature side: $T_{neutron}$ = 195 K, $T_{uranium}$ = 188 K. This can be caused by the oxygen interstitial localized next to the Be^{2+} ion: $Be^{2+}O^{-} + O_i^0 \rightarrow Be^{2+}O_2^{-}$, hence increasing the potential well of the $[Be]^{+}$ centre and lowering the temperature of centre thermal destruction.

The well-known radiation resistivity of pure MgO crystals has to be re-investigated in the light of the recent measurements on anion vacancy and interstitial formation and stabilization. New effective mechanisms of energy dissipation of hot charge carriers have to be discovered, probably by means of doping of different impurities into pure MgO crystals.

SUMMARY

In a close-packed MgO crystal with the ionic radii ratio of oxygen O^{2-} and Mg^{2+} ions $r_{O^{2-}}/r_{Mg^{2+}} \approx 2$, the formation energy of a Frenkel pair exceeds the energy gap E_g. Because of this, the creation of defects via the recombination of non-relaxed (cold) electrons and hole is impossible, resulting in a sufficiently high resistance of MgO, widely used for various technical applications, against X- or γ-rays. However, the peculiarities of electron-hole and interstitial-vacancy processes under the irradiation of wide-gap materials by fast neutrons and swift ions are to be investigated in detail in order to increase the radiation resistance of MgO, Al_2O_3 etc. needed for future thermonuclear (fusion) energetics. The aim of this thesis was to describe the variety of different possible hole and interstitial centres in pure and doped with various impurities MgO single crystals. Their formation, optical properties, thermal release of charge carriers and luminescence were presented.

The analysis of different stabilization factors for the hole centres was done in sight of a hole self-trapping problem in pure MgO single crystals. It was assumed that a hole self-trapping on an oxygen ion can happen only next to lattice distortions caused by either cation vacancy, possibly vacancy complexes (according to one of the interpretations of 2.9 eV "blue" luminescence) or an impurity ion substituting the Mg^{2+} ion. It has been shown that V-type centres are stable up to 420 K (V^- centre) with a cation vacancy being the main stabilization factor. The V^-, V^0, V_{OH}, and V_{Al} centres have a similar structure with a slight perturbation by an impurity ion for the latter two centres, which is manifested in the close absorption band peaks at 2.2–2.4 eV.

A new V-type centre was discovered in Be-doped MgO single crystals, the $V_{OH\text{-}Be}$ centre ($Be^{2+} – O^- – v_c – OH^-$), which is stable up to 400 K, which is much higher than for V_{OH} centre. This showed another stabilization factor besides the cation vacancy, namely the electric dipole caused by an outward relaxation of the Be^{2+} ion from the central Mg^{2+} lattice site due to the small ionic radius of the former. Such perturbation increases the energy gap between the ground and the first allowed excited state of the localized hole visible in the absorption spectrum at 3.2 eV.

Another hole centre was discovered in MgO:Be single crystals, the $[Be]^+$ ($Be^{2+} – O^-$) centre. The centre has rhombic symmetry, although the distortion from the tetragonal symmetry is very small. The EPR spectrum of this centre can be observed up to 40 K and its thermal destruction occurs at ~195 K. Although the centre has a structure, similar to the $[Li]^0$ and $[Na]^0$ centres, the hole localization mechanism is proved to be

different. In the latter case, it is a Columbic interaction due to an excess negative charge at the Mg^{2+} central lattice site (Li and Na are monovalent), while for the former, the stabilization factor is the electric dipole, created in the same way as for $V_{OH\text{-}Be}$ centre. As Be and Mg are isovalent, these discoveries are a step forward in understanding the absence of self-trapping of the holes in pure MgO. It was assumed that there exists a $[Ca]^+$ centre in Ca-doped MgO single crystals possessing a $[Be]^+$ structure, which can be formed by crystal irradiation at $T < 30$ K. A TL peak in MgO:Ca was observed at 48 K and was assigned to such centre. Due to technical limitations, the EPR spectrum could not be measured for $[Ca]^+$. The discovery of the $[Ca]^+$ centre by means of EPR is the next step in the experimental understanding of the self-trapping problem in wide gap dielectrics.

The significance of a novel non-impact mechanism of formation and stabilization of interstitial oxygen centres was confirmed. The high density of the electronic excitations formed in the tracks of swift heavy ions drastically increases the probability of hot electron-hole recombination with an energy release, sufficient for creating Frenkel defects. The comparison of the CL measured for the MgO crystals, irradiated by fast neutrons and by swift heavy ^{238}U ions, showed an intensity increase of F^+ centres compared to F centres which means there is a high concentration of anion vacancies v_a which serve as efficient radiative traps for the electrons. This is an indirect evidence of the high concentration of stabilized oxygen interstitials. A peak at 695 K in the TL of SHI irradiated MgO crystals also proves this.

An evidence of interstitial localization next to $[Be]^+$ centre was observed. The $[Be]^+$ centre can serve as a source for neutral oxygen capture and H centre formation at low temperatures. This is possible due to the small ionic radius of the Be^{2+} ion and its non-central position in the MgO lattice.

SUMMARY IN ESTONIAN

AUK- JA INTERSTITSIAALTSENTRID KIIRITUSKINDLATES MgO MONOKRISTALLIDES

Tihedalt pakitud MgO kristallides, kus anioonide (O^{2-}) ja katioonide (Mg^{2+}) raadiuste suhe on lähedane 2-le, on Frenkeli defektide tekitamise energia $E_{FD} > E_g$, mis muudab Frenkeli defektide tekke relakseerunud (külmade) elektronide ja aukude rekombinatsioonil võimatuks ning paljudes rakendustes tagab MgO kõrge kiirituspüsivuse röntgen- ja γ-kiirguse suhtes. Kuid laia keelupiluga MgO, Al_2O_3 jt kasutamine termotuumaenergeetikas nõuab elektron-auk- ja interstitsiaal-vakantsprotsesside eripära uurimist ka keerulisemate kiiritusliikide – kiired neutronid ja ioonid – korral ning nende kiirituspüsivuse edasist tõstmist.

Käesoleva väitekirja eesmärgiks oli kirjeldada erinevaid auk- ja interstitsiaaltsentreid puhtais ja mitmete lisanditega legeeritud MgO kristallides. Vaadeldakse nende teket, struktuuri, optilisi omadusi, termilist lagunemist ja luminestsentsi.

Analüüsiti auktsentrite stabilisatsioonitegureid, pidades silmas aukude autolokalisatsiooni probleemi puhatas MgO-s. Eeldati, et aukude haaramine hapniku ioonile saab toimuda ainult katioonvakantsi, vakantsikompleksi (vastavalt 2.9 eV luminestsentsi ühele tõlgendusele) või Mg^{2+} iooni asendava katioonlisandi põhjustatud häirituse olemasolul. On näidatud, et V-tüüpi auktsentrid on stabiilsed temperatuurini 420 K (V^- tsenter), kusjuures peamine stabilisatsioonitegur on neis sisalduv katioonvakants. V^-, V^0, V_{OH} ja V_{Al} tsentreil on ühesugune struktuur, väikese lähedalasuvast lisandioonist põhjustatud täiendava häiritusega viimasel kahel juhul, mis väljendub nende optiliste neeldumisribade läheduses (2.2–2.4 eV).

Be-lisandiga MgO kristallides avastati uus V-tüüpi tsenter: $V_{OH\text{-}Be}$ ($Be^{2+} – O^- – v_c – OH^-$), mis on stabiilne temperatuurini 400 K, seega tunduvalt stabiilsem kui V_{OH} tsenter (335 K). See annab tunnistust teisest stabilisatsioonitegurist, lisaks katioonvakantsile, nimelt Mg^{2+} võresõlmes paikneva väikese ioonraadiusega Be^{2+} relaksatsioonil tekkinud elektrilisest diipolist. Selline häiritus suurendab energiapilu põhi- ja esimese ergastatud seisundi vahel, mis avaldub optilise neeldumise nihkega 3.2 eV juurde.

Teine MgO:Be monkristallis avastatud uus auktsenter oli $[Be]^+$ ($Be^{2+} – O^-$) centre. Tsetnri sümmeetria on rombiline, ehkki kõrvalekalle tetragonaalsest on väike. Tsentri EPR spekter on jälgitav kuni 40 K-ni (ülemine piir) ning tema termiline lagunemine toimub ~195 K juures.

12

Kuigi tsenter sarnaneb struktuurilt $[Li]^0$ ja $[Na]^0$ tsentereile, on tema augu lokaliseerumise mehhanism erinev. $[Li]^0$ ja $[Na]^0$ korral on see Mg^{2+} võresõlmes paikneva efektiivse negatiivse laengu (Li ja Na on ühevalentsed) kuloniline vastasmõju, kuna $[Be]^+$ korral on stabilisatsiooniteguriks, nii nagu $V_{OH\text{-}Be}$ tsentri juhulgi, elektriline diipol. Kuna Be ja Mg on isovalentsed, tõstatab leitud tsenter küsimuse aukude autolokalisatsioonist MgO-s. Veelgi väiksemat augu lokalisatsioonile viivat häiritust on oodata $[Ca]^+$ tsentrite korral, mille olemasolu on mitmes töös eeldatud. $[Ca]^+$ tsentri struktuur on sarnane $[Be]^+$ tsentri omale, ta tekib kristalli kiiritamisel $T < 30$ K juures. Tema termilise lagunemisega seostatakse TL piiki temperatuuril 48 K. Tehniliste probleemide tõttu ei ole $[Ca]^+$ EPR meetodil veel tuvastatud.

Uurimused kinnitasid aniooninterstitsiaalide tekke- ja stabilisatsiooni uue, mittepõrkemehhanismi olulisust MgO-s. Kiirete raskete ioonide jälgedes tekkivate elektronergastuste suur tihedus suurendab järsult Frenkeli defektide tekkele viivate kuumade elektron-auk-rekombinatsioonide tõenäosust. Kiirete neutronite ja kiirete raskete ^{238}U ioonidega pommitatud MgO kristallide katoodluminestsentsi võrdlev uurimus näitas, et viimastes on F^+ tsentrite luminestsentsi osakaal F tsentrite omaga võrreldes oluliselt intensiivsem, mis tähendab, et ^{238}U-ga pommitamine tekitas hulgaliselt anioonvakantse v_a , millede poolt elektroni haaramine tekitabki F^+ – luminestsentsi. See annab kaudselt tunnistust suure kontsentratsiooniga stabiliseeritud interstitsiaalide olemasolust uraaniga kiiritatud kristallides. Seda kinnitab ka 695 K piik kiirete raskete ioonidega kiiritatud MgO TL spektreis.

Tuvastati interstitsiaalide lokaliseerumine $[Be]^+$ kõrval. $[Be]^+$ võib haarata neutraalseid hapniku aatomeid ning aidata madalal temperatuuril kaasa H-tsentrite (O_2^-) moodustumisele. See on võimalik Be^{2+} iooni väikese raadiuse ning tema mittetsentraalse asendi tõttu MgO võres.

APPENDIX A

In the context of this work, an EPR simulation software, called VirtualEPR Spectrometer, was created. Its main objective is the EPR spectrometer simulation for both scientific and educational purposes. This includes:

- Storing/Loading data for different crystals and defects
- EPR spectrum simulation for all possible defect configurations including interaction of several electronic and nuclear spins
- Spectrum dependence on the microwave frequency and crystal orientation with respect to the direction of a static magnetic field
- Spectrum intensity dependence on temperature and microwave power
- The so-called Educational mode

The last term probably describes the most valuable usage of the VirtualEPR Spectrometer. In this mode, users can access simulated defect parameters only by using the password. The supervisor can give a task to interpret the given EPR spectrum (which can actually consist of several added spectra in the same crystal, i.e. recreating a close to real situation). Optional parameterization of the spectrum angular, thermal and microwave power dependencies simulates realistic spectrum measurements, hence, introducing a full power of magnetic resonance to the students.

Theoretical calculations of an EPR spectrum can be done using either perturbation theory or exact diagonalization of SH matrix. As the former gives quite rough estimates for EPR transition energies, the latter approach was chosen in the VirtualEPR Spectrometer software. The down side of such approach is a high calculation time.

A.1. Spin Hamiltonian matrix

The general form of SH can be given with the following equation:

$$\hat{H} = \beta\vec{\mathbf{B}}\mathbf{g}\hat{\mathbf{S}} + h\hat{\mathbf{S}}\mathbf{D}\hat{\mathbf{S}} + h\sum_{m=-4}^{4} B_4^m O_4^m(S) + h\sum_{m=-6}^{6} B_6^m O_6^m(S) +$$

$$+ \sum_{i=1}^{n}\left(h\hat{\mathbf{S}}\mathbf{A}_i\hat{\mathbf{I}}_i - g_{N_i}\beta_N\vec{\mathbf{B}}\hat{\mathbf{I}}_i + h\hat{\mathbf{I}}_i\mathbf{Q}_i\hat{\mathbf{I}}_i + h\sum_{m=-4}^{4}\left(B_4^m\right)_i O_4^m(I_i) + h\sum_{m=-6}^{6}\left(B_6^m\right)_i O_6^m(I_i)\right),$$

where n is the number of nuclear spins, B_4^m and B_6^m are the octupole and hexadecapole interaction parameters, respectively, O_4^m and O_6^m are Stevens operators, which depend on the spin value, and the rest of the parameters are known from equation (2).

The angular and symmetry dependence of the SH is introduced via the magnetic field vector $\vec{B} = \{B_x, B_y, B_z\}$: before the SH calculation vector is multiplied on a crystal orientation matrix and then on a symmetry element matrix.

The terms in the SH are represented either as a vector-matrix or as a scalar-matrix multiplication. The sizes of the resulting matrices can vary. In order to bring them all to a common size the outer multiplication is used by the following rules:

- Every electron term with spin S is outer multiplied from the right on the unity matrix of size $\prod_{i=1}^{n} I_i$
- Every i^{th} nuclear term with spin I_i related is outer multiplied from the left on the unity matrix of size $S \cdot \prod_{j=1}^{i-1} I_j$ and outer multiplied from the right on the unity matrix of size $\prod_{j=i+1}^{n} I_j$

These rules will produce an SH matrix of size $S \cdot \prod_{i=1}^{n} I_i$, which is a hermitian matrix with, in general, non-zero imaginary part. One of the properties of hermitian matrices is that they can be always diagonalized, which means is that there exist matrix U and diagonal matrix D, and that the following applies:

$$UDU^{-1} = SH.$$

The diagonal elements of matrix D, d_{ii}, are called the eigenvalues, while the vector columns of matrix U, u_i, are the eigenvectors of eigenvalue d_{ii}.

A.2. Calculation of the EPR absorption band position

As it was stated in the previous chapter, the SH matrix is diagonalizable. Hence, the SH matrix diagonalization produces exact EPR transition energies E_i (eigenvalues) and the coefficients of the basis wave function, c_i (eigenvectors). The product of the eigenvector on its transpose gives the probability, i.e. intensity, of the EPR absorption band:

$$I = c_i c_i^T.$$

Unfortunately, in the simulation the unknown parameter is the static magnetic field (in the field-swept EPR experiment), with the transition energy known in advance from the microwave frequency $h\upsilon = E_i - E_j$. The consequence of this is that the SH matrix fitting must be done for

every allowed EPR transition $i \to j$ with the magnetic field as a varying parameter. In the VirtualEPR Spectrometer, the least-square fitting is used with a view to minimize the value of the following function:

$$S = \sum_i \frac{(\mathrm{f}(x_i, \vec{\mathbf{a}}) - F_i)^2}{\sigma_i^2},$$

where $\mathrm{f}(x_i, \vec{\mathbf{a}})$ is a fitting function value at x_i, F_i – experimental value, σ_i – the weighting factor, and $\vec{\mathbf{a}}^T = (a_1, a_2, ..., a_n)$ – is the collection of varied parameters. Every fitting step results in the determination of the next possible value for the varied parameters:

$$a_i^{m+1} = a_i^m - \left(\frac{\partial S}{\partial a_i}\right)\left(\frac{\partial^2 S}{\partial a_i^2}\right)^{-1},$$

where derivatives are calculated at a_i^m.

For the SH matrix, the fitting function is $\Delta E(\vec{B}) = \langle \varphi_i^* | \hat{H} | \varphi_i \rangle - \langle \varphi_j^* | \hat{H} | \varphi_j \rangle$ with the experimental value $h\upsilon$. Hence, the partial derivatives of S will look like this:

$$\frac{\partial S}{\partial B} = \frac{\Delta E}{|\Delta E|}\left(|\Delta E| - h\nu\right)\left(\frac{\partial E_i}{\partial B} - \frac{\partial E_j}{\partial B}\right) \quad \text{and}$$

$$\frac{\partial^2 S}{\partial B^2} = \left(\frac{\partial E_i}{\partial B} - \frac{\partial E_j}{\partial B}\right)^2 + \frac{\Delta E}{|\Delta E|}\left(|\Delta E| - h\nu\right)\left(\frac{\partial^2 E_i}{\partial B^2} - \frac{\partial^2 E_j}{\partial B^2}\right)$$

To calculate these derivatives, one must apply the Feynman's theorem, which states that the derivative of the energy with respect to the SH parameter equals to the expectation value of the derivative of the SH. Hence,

$$\frac{\partial E_i}{\partial B} = \langle \varphi_i | \frac{\partial \hat{H}}{\partial B} | \varphi_i \rangle \text{ and } \frac{\partial^2 E_i}{\partial B^2} = \sum_j \frac{\langle \varphi_i | \frac{\partial \hat{H}}{\partial B} | \varphi_j \rangle \langle \varphi_j | \frac{\partial \hat{H}}{\partial B} | \varphi_i \rangle}{E_i - E_j} + c.c.,$$

where j goes through all the energy levels and *c.c.* stands for the complex conjugate. Finally, in a computer usable format, these derivatives can be written in the following way:

$$\frac{\partial E_i}{\partial B} = Tr\left[\frac{\partial H}{\partial B} c_i \otimes c_i^T\right] \text{ and } \frac{\partial^2 E_i}{\partial B^2} = \sum_j Tr\left[\frac{\left(\frac{\partial H}{\partial B}\right)^2 \left(c_i \otimes c_i^T\right)\left(c_j \otimes c_j^T\right)}{E_i - E_j}\right] + c.c.,$$

where $E_{i,j}$ are SH eigenvalues and $c_{i,j}$ are their eigenvectors.

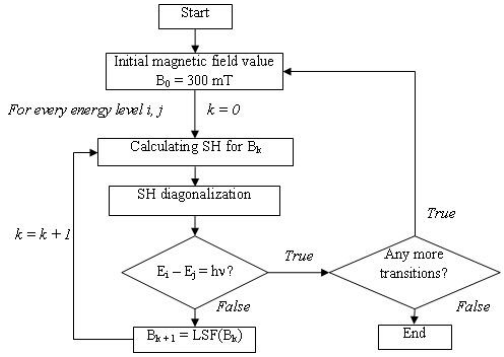

Figure 27. Algorithm of EPR spectrum simulation

At this point, it is obvious that the calculation of the magnetic field position for every transition $i \to j$ requires $n(n+1)/2$ least square fitting runs. As every fitting step requires matrix diagonalization and calculation of SH derivatives, this is obviously a time consuming problem. Taking into account only the allowed EPR transitions with $\Delta M_S = 1$, which can be achieved by a proper extension of every SH term to the SH matrix size, time consumption can be substantially reduced. The general algorithm of locating EPR transitions is given in Fig 24.

A.3. EPR band linewidth and intensity

As it was shown above, the EPR band linewidth and intensity can be calculated theoretically using (8) and (9). For that, the spin-spin relaxation time τ_2 and parameters of Kronig-van Fleck mechanism (7) a, b, c, n and Δ must be specified. Given these parameters, the VirtualEPR Spectrometer provides that functionality, hence, the dependence on temperature and microwave power (including saturation processes) can be easily reproduced knowing the experimental values for these parameters. This is of great importance for educational purposes, when the complete behaviour of the real EPR spectrometer is simulated.

REFERENCES

[1] A. Ibarra, E. R. Hodgson, "The ITER project: the role of insulators", *Nucl. Instr. and Meth. in Phys. Res. B*, **218**, 29, 2004

[2] J. Werz, J. Bolton, "Теория и практическое приложение метода ЭПР", *Мир*, Москва, 1975

[3] O. F. Schirmer, "Trapped-hole center containing lithium in MgO, CaO and SrO", *J. Phys. Chem. Sol.*, **32**, 499, 1971

[4] M. M. Abraham, W. P. Unruh, Y. Chen, "Electron-nuclear-double-resonance investigations of [Li]0 and [Na]0 centers in MgO, CaO and SrO", *Phys. Rev. B*, **10**, 3540, 1974

[5] O. F. Schirmer, K. W. Blazey, W. Berlinger, "ESR and optical absorption of bound-small polarons in YAlO3", *Phys. Rev. B*, **11**, 4201, 1974

[6] O. F. Schirmer, "O- bond small polarons in oxide materials", *J. Phys: Condens. Matter*, **18**, R667, 2006

[7] M. J. Norgett, A. M. Stoneham, A. P. Pathak, "Electronic structure of the V- center in MgO", *J. Phys. C Solid*, **10**, 555, 1977

[8] A. Abraham, B. Bleany, "Электронный парамагнитный резонанс переходных ионов", *Мир*, Москва, 1972

[9] Y. Chen, M. M. Abraham, "Trapped-hole centers in alkaline-erath oxides", *J. Phys. Chem. Solids*, **51**, 747, 1990

[10] R. G. Wyckoff, "Crystal Structures", *Wiley*, New York , 1963

[11] G. Pechham, "The phonon dispersion relation for magnesium oxide", *Proc. Phys. Soc.*, **90**, 657, 1967

[12] J. B. Bates, M. H. Brooker, "Determination of longitudinal optical mode frequencies by polarized specular reflectance infrared spectroscopy", *Phys. Chem. Sol.*, **32**, 2403, 1971

[13] G. Pacchioni, "Measures of ionicity of alkaline-earth oxides from the analysis of ab initio cluster wave functions", *Phys. Rev. B*, **48**, 11573, 1993

[14] R. D. Shannon, "Revised effective ionic radii and systematic studies of interatomic distances in halides and chalcogenides", *Acta. Cryst.*, **A32**, 751, 1976

[15] D. M. Roessler, W. C. Walker, "Electronic spectrum and ultraviolet optical properties of crystalline MgO", *Phys. Rev.*, **159**, 733, 1967

[16] R. C. Whited, W. C. Walker, "Exciton spectra of CaO and MgO", *Phys. Rev. Let.*, **22**, 1428, 1969

[17] U. Schönberger, F. Aryasetiwan, "Bulk and surface electronic structures of MgO", *Phys. Rev. B*, **52**, 8788, 1995

[18] V. A. Sashin, H. E. Dorsett, M. A. Bolorizadeh, M. J. Ford, "The valence band structures of BeO, MgO and CaO", *J. Chem. Phys.*, **113**, 8175, 2000

[19] J. E. Wertz, P. Auzins, J. H. Griffiths, J. W. Orton, "Spin resonance studies of defects in magnesium oxide", *Discuss. Faraday Soc.*, **28**, 136, 1959

[20] Y. Chen, M. M. Abraham, W. P. Unruh, "Formation and stability of V- and VAl centers in MgO", *Phys. Rev. B*, **9**, 1842, 1973

[21] T. Kärner, A. F. Malysheva, A. Maaroos, V. V. Murk, *Sov. Phys. Solid State*, **22**, 1178, 1980

[22] L. A. Kappers, F. Dravnieks, J. E. Wertz, *Solid State Commun.*, **10**, 1265, 1972

[23] Y. Chen, M. M. Abraham, L. C. Templeton, W. P. Unruh, "Role of hydrogen and deuterium on the V- center formation in MgO", *Phys. Rev. B*, **11**, 881, 1974

[24] B. Henderson, J. E. Wertz, "Defects in the Alkaline Earth Oxides", *Taylor&Francis*, London, 1979

[25] L. A. Kappers, F. Dravnieks, J. E. Wertz, "Electron spin resonance and optical studies of the double-hole (V0) center in MgO", *J. Phys. Sol. State*, **7**, 1387, 1974

[26] S. A. Dolgov, T. Kärner, T. I. Savihhina, B. T. Tazhigulov, *Trudy IF Akad. Nauk. Est. SSR*, **61**, 139, 1987

[27] M.M. Abraham, Y. Chen, "Stable [Li]0 defects in MgO single crystals", *Phys. Rev. Let.*, **37**, 849, 1976

[28] M. M. Abraham, Y. Chen, J. L. Kolopus, H. T. Tohver, "Radiation-induced [Na]0 centers in MgO and SrO",

[29] A. Maaroos, *Trudy IF Akad. Nauk. Est. SSR*, **53**, 49, 1982

[30] I. E. Lacis, J. A. Valbis, *Phys. Status Solidi B*, **95**, K21, 1979

[31] W. C. Mackrodt, R. F. Stewart, "Defect properties of ionic solids. III. The calculation of the point-defect structure of the alkaline-earth oxides and CdO", *J. Phys. C: Solid State Phys.*, **12**, 5015, 1979

[32] J. R. Morton, K. F. Preston, "Atomic parameters for paramagnetic resonance data", *J. Magn. Reson.*, **30**, 577, 1978

[33] Z. A. Rachko, J. A. Valbis, "Luminescence of Free and Relaxed Excitons in MgO", *Phys. Stat. Sol. (b)*, **93**, 161, 1979

[34] A. L. Shluger, R. W. Grimes, C. A. Catlow, N. Itoh, "Self-trapping holes and excitons in the bulk and on the (100) surface of MgO", *J. Phys.: Condens. Matter*, **3**, 8027, 1991

[35] M. Elango, T. Pruulmann, A. P. Zhurakovskii, "Recombination luminescence and energy transfer in ionic crystals at XUV excitation by synchrotron radiation", *Phys Status Solidi (b)*, **115**, 399, 1983

[36] E.. Kh.. Feldbakh, Ch. B. Lushchik, I. L. Kuusmann, "Coexistance of large- and small-radius excitons bound on defects in solids", *JETP Lett.*, **39**, 61, 1984

[37] L. E. Halliburton, L. A. Kappers, "Radiation-induced oxygen interstitials in MgO", *Solid State Comm.*, **26**, 111, 1978

[38] T. Kärner, S. Dolgov, A. Lushchik, N. Mironova-Ulmane, S. Nakonechnyj, E. Vasil'chenko, "High-temperature thermoluminescence manifestations of anion interstitials in neutron-irradiated pure and doped single crystals of MgO", *Rad. Eff. Def. Sol.*, **155**, 171, 2000

[39] T. Kärner, S. Dolgov, N. Mironova-Ulmane, S. Nakonechnyj, E. Vasil'chenko, "Anion interstitials in neutron-irradiated MgO single crystals", *Rad. Meas.*, **33**, 625, 2001

[40] T. Kärner, S. Dolgov, A. Lushchik, N. Mironova-Ulmane, S. Nakonechnyj, A. Maaroos, "Thermoluminescence centers created selectively in MgO crystals by fast neutrons", *Rad. Prot. Dosim.*, **100**, 127, 2002

[41] W. Känzig, M. H. Cohen, "Paramagnetic Resonance of Oxygen in Alkali Halides", *Phys. Rev. Let.*, **3**, 509, 1959

[42] G. H. Rosenblatt, M. W. Rowe, G. P. Williams, R. T. Williams, Y. Chen, "Luminescence of F and F+ centers in magnesium oxide", *Phys. Rev. B*, **39**, 10310, 1988

[43] J. M. Luthra, A. Sathyamoorthy, N. M. Gupta, "A thermoluminescence study of defect centers in MgO", *J. Lumin.*, **15**, 395, 1977

[44] E. Vasil'chenko, A. Lushchik, Ch. Lushchik, *Sov. Phys. Solid State*, **12**, 167, 1970

14

ACKNOWLEDGEMENTS

I have a great pleasure to thank everybody who have worked with me and helped me physically and morally to get to the finish line of the 10-year educational sprint.

I express my sincere gratitude to my supervisor Ph.D. Tiit Kärner who has always believed in me and supported me. His priceless advice made this thesis come true.

Tender thanks to my supervisor, D. Sc., Prof. Aleksandr Lushchik, Head of Laboratory of Physics of Ionic Crystals, for his continuous support and help in finishing this thesis. I am grateful to him for bringing me first to the world of EPR spectroscopy and solid state physics.

I would like to thank D. Sc. Aleksandr Shluger and Ph. D. Peter Sushko, London Centre for Nanotechnology, for the possibility to work in the field of computer modelling of the defects in insulators.

I report my acknowledgements to the Estonian Science Foundation for the financial support during all these years.

I would like to say special words of gratitude to my parents, who always pushed me forward, and to my wife and daughter for their love and indispensable support.

PUBLICATIONS

I

S. A. Dolgov, V. Issahhanjan, T. Kärner, A. Maaroos, S. Nakonechnyi
"VOH-Be – a new and unusual member in the family of V centres"
J. Phys.: Condens. Matter, 14, 8881–8888, 2002

II

S. A. Dolgov, V. Issahhanjan, T. Kärner, A. Maaroos, S. Nakonechnyi
"Electron paramagnetic resonance of the $[Be]^{+}$ centre in MgO:Be"
J. Phys.: Condens. Matter, **15**, 6871–6878, 2003

III

T. Kärner, S. A. Dolgov, V. Issahhanjan, A. Maaroos, S. Nakonechnyi
"Paramagnetic centres in Be-doped MgO single crystals"
Rad. Eff. Def. Sol., **185**, 163–166, 2003

IV

S. A. Dolgov, V. Issahhanjan, T. Kärner, P. Liblik,
A. Maaroos, S. Nakonechnyi
"Luminescence of [Be]+ centre in MgO:Be"
Rad. Meas, **38**, 699–702, 2004

V

V. Issahhanjan, T. Kärner, A. Maaroos, S. Nakonechnyi
"Spin relaxation processes in the defect hole
of Be-doped MgO single crystals"
Phys. Stat. Sol. (c), **2**, 426–429, 2005

VI

A. Lushchik, T. Kärner, Ch. Lushchik, E. Vasil'chenko, S. Dolgov,
V. Issahhanjan, P. Liblik "Dependence of long-lived defect
creation on excitation density in MgO single crystals"
Phys. Stat. Sol. (c), **4 (3)**, 1084–1087, 2007

VII

A. Lushchik, Ch. Lushchik, K. Schwartz, E. Vasil'chenko,
T. Kärner, I. Kudryavtseva, V. Issahhanjan, A. Shugai
"Stabilization and annealing of interstitials formed
by radiation in binary metal oxides and fluorides"
Nucl. Instr. And Meth. B, **266**, 2868–2871, 2008

CURRICULUM VITAE

Name:	Vigen Issahhanjan
Data and place of birth:	August 30, 1980, Armenia
Citizenship:	Estonian
Address:	Institute of Physics, University of Tartu Riia str. 142, 51014 Tartu, Estonia
Phone:	+372 529 3198
E-mail:	vigen@fi.tartu.ee

Education:	1998, Narva Pähklimäe Gümnaasium 1998 – 2002, University of Tartu, Department of Physics and Chemistry, B.Sc. in Physics 2002 – 2004, University of Tartu, Department of Physics and Chemistry, M.Sc. in Solid State Physics 2004 – …, University of Tartu, Department of Physics and Chemistry, Ph.D. student
Professional development:	2004, International School in Radiation Effects in Solids, NATO-ASI Course, Erice, Italy 2005, University College London, Condensed Matter and Materials Physics, London, UK
Employment:	2003 – 2004, University of Tartu, Engeneer 2005 – 2007, University of Tartu, Doctoral School of Material Science and Material Technology, extraordinary researcher 2004 – 2006, FieldForce Solution OY, Software developer 2006 – …, Skype Technologies OÜ, Software developer
Publications:	7 scientific articles, 2 posters, 4 conference contributions

ELULUGU

Nimi:	Vigen Issahhanjan
Sünniaeg ja -koht:	30.08.1980, Armeenia
Kodakonsus:	Eesti
Aadress:	Füüsika Instituut, Tartu Ülikool Riia 142, 51014 Tartu, Eesti
Telefon:	+372 529 3198
E-post:	vigen@fi.tartu.ee

Haridus:	1998, Narva Pähklimäe Gümnaasium 1998 – 2002 Tartu Ülikool, Füüsika-Keemia teaduskond, B.Sc. Füüsikas 2002 – 2004, Tartu Ülikool, Füüsika-Keemia teaduskond, M.Sc. Tahkise Füüsikas 2004 – …, Tartu Ülikool, Füüsika-Keemia teaduskond, doktorant
Erialane enesetäiendus:	2004, International School in Radiation Effects in Solids, NATO-ASI Course, Erice, Italy 2005, University College London, Condensed Matter and Materials Physics, London, UK
Teenituskäik:	2003 – 2004, Tartu Ülikool, Insener 2005 – 2006, Tartu Ülikool, Materjaliteaduse ja Materjalide Tehnoloogia Doktorikool, Erakorraline teadur 2004 – 2006, FieldForce Solution OY, Programmeerija 2006 – …, Skype Technologies OÜ, Programmeerija
Publikatsioonid:	7 teaduslikku publikatsiooni, 2 postrit, 4 konferentsi kaasaitamine

DISSERTATIONES PHYSICAE UNIVERSITATIS TARTUENSIS

1. **Andrus Ausmees.** XUV-induced electron emission and electron-phonon interaction in alkali halides. Tartu, 1991.
2. **Heiki Sõnajalg.** Shaping and recalling of light pulses by optical elements based on spectral hole burning. Tartu, 1991.
3. **Sergei Savihhin.** Ultrafast dynamics of F-centers and bound excitons from picosecond spectroscopy data. Tartu, 1991.
4. **Ergo Nõmmiste.** Leelishalogeniidide röntgenelektronemissioon kiiritamisel footonitega energiaga 70–140 eV. Tartu, 1991.
5. **Margus Rätsep.** Spectral gratings and their relaxation in some low-temperature impurity-doped glasses and chrystals. Tartu, 1991.
6. **Tõnu Pullerits.** Primary energy transfer in photosynthesis. Model calculations. Tartu, 1991.
7. **Olev Saks.** Attoampri diapasoonis voolude mõõtmise füüsikalised alused. Tartu, 1991.
8. **Andres Virro.** AlGaAsSb/GaSb heterostructure injection lasers. Tartu, 1991.
9. **Hans Korge.** Investigation of negative point discharge in pure nitrogen at atmospheric pressure. Tartu, 1992.
10. **Jüri Maksimov.** Nonlinear generation of laser VUV radiation for high-resolution spectroscopy. Tartu, 1992.
11. **Mark Aizengendler.** Photostimulated transformation of aggregate defects and spectral hole burning in a neutron-irradiated sapphire. Tartu, 1992.
12. **Hele Siimon.** Atomic layer molecular beam epitaxy of A^2B^6 compounds described on the basis of kinetic equations model. Tartu, 1992.
13. **Tõnu Reinot.** The kinetics of polariton luminescence, energy transfer and relaxation in anthracene. Tartu, 1992.
14. **Toomas Rõõm.** Paramagnetic H^{2-} and F^+ centers in CaO crystals: spectra, relaxation and recombination luminescence. Tallinn, 1993.
15. **Erko Jalviste.** Laser spectroscopy of some jet-cooled organic molecules. Tartu, 1993.
16. **Alvo Aabloo.** Studies of crystalline celluloses using potential energy calculations. Tartu, 1994.
17. **Peeter Paris.** Initiation of corona pulses. Tartu, 1994.
18. **Павел Рубин.** Локальные дефектные состояния в CuO_2 плоскостях высокотемпературных сверхпроводников. Тарту, 1994.
19. **Olavi Ollikainen.** Applications of persistent spectral hole burning in ultrafast optical neural networks, time-resolved spectroscopy and holographic interferometry. Tartu, 1996.
20. **Ülo Mets.** Methodological aspects of fluorescence correlation spectroscopy. Tartu, 1996.
21. **Mikhail Danilkin.** Interaction of intrinsic and impurity defects in CaS:Eu luminophors. Tartu, 1997.

28

22. **Ирина Кудрявцева.** Создание и стабилизация дефектов в кристаллах KBr, KCl, RbCl при облучении ВУФ-радиацией. Тарту, 1997.
23. **Andres Osvet.** Photochromic properties of radiation-induced defects in diamond. Tartu, 1998.
24. **Jüri Örd.** Classical and quantum aspects of geodesic multiplication. Tartu, 1998.
25. **Priit Sarv.** High resolution solid-state NMR studies of zeolites. Tartu, 1998.
26. **Сергей Долгов.** Электронные возбуждения и дефектообразование в некоторых оксидах металлов. Тарту, 1998.
27. **Kaupo Kukli.** Atomic layer deposition of artificially structured dielectric materials. Tartu, 1999.
28. **Ivo Heinmaa.** Nuclear resonance studies of local structure in $RBa_2Cu_3O_{6+x}$ compounds. Tartu, 1999.
29. **Aleksander Shelkan.** Hole states in CuO_2 planes of high temperature superconducting materials. Tartu, 1999.
30. **Dmitri Nevedrov.** Nonlinear effects in quantum lattices. Tartu, 1999.
31. **Rein Ruus.** Collapse of 3d (4f) orbitals in 2p (3d) excited configurations and its effect on the x-ray and electron spectra. Tartu, 1999.
32. **Valter Zazubovich.** Local relaxation in incommensurate and glassy solids studied by Spectral Hole Burning. Tartu, 1999.
33. **Indrek Reimand.** Picosecond dynamics of optical excitations in GaAs and other excitonic systems. Tartu, 2000.
34. **Vladimir Babin.** Spectroscopy of exciton states in some halide macro- and nanocrystals. Tartu, 2001.
35. **Toomas Plank.** Positive corona at combined DC and AC voltage. Tartu, 2001.
36. **Kristjan Leiger.** Pressure-induced effects in inhomogeneous spectra of doped solids. Tartu, 2002.
37. **Helle Kaasik.** Nonperturbative theory of multiphonon vibrational relaxation and nonradiative transitions. Tartu, 2002.
38. **Tõnu Laas.** Propagation of waves in curved spacetimes. Tartu, 2002.
39. **Rünno Lõhmus.** Application of novel hybrid methods in SPM studies of nanostructural materials. Tartu, 2002.
40. **Kaido Reivelt.** Optical implementation of propagation-invariant pulsed free-space wave fields. Tartu, 2003.
41. **Heiki Kasemägi.** The effect of nanoparticle additives on lithium-ion mobility in a polymer electrolyte. Tartu, 2003.
42. **Villu Repän.** Low current mode of negative corona. Tartu, 2004.
43. **Алексей Котлов.** Оксианионные диэлектрические кристаллы: зонная структура и электронные возбуждения. Tartu, 2004.
44. **Jaak Talts.** Continuous non-invasive blood pressure measurement: comparative and methodological studies of the differential servo-oscillometric method. Tartu, 2004.
45. **Margus Saal.** Studies of pre-big bang and braneworld cosmology. Tartu, 2004.

46. **Eduard Gerškevitš.** Dose to bone marrow and leukaemia risk in external beam radiotherapy of prostate cancer. Tartu, 2005.
47. **Sergey Shchemelyov.** Sum-frequency generation and multiphoton ionization in xenon under excitation by conical laser beams. Tartu, 2006.
48. **Valter Kiisk.** Optical investigation of metal-oxide thin films. Tartu, 2006.
49. **Jaan Aarik.** Atomic layer deposition of titanium, zirconium and hafnium dioxides: growth mechanisms and properties of thin films. Tartu, 2007.
50. **Astrid Rekker.** Colored-noise-controlled anomalous transport and phase transitions in complex systems. Tartu, 2007.
51. **Andres Punning.** Electromechanical characterization of ionic polymer-metal composite sensing actuators. Tartu, 2007.
52. **Indrek Jõgi.** Conduction mechanisms in thin atomic layer deposited films containing TiO_2. Tartu, 2007.
53. **Aleksei Krasnikov.** Luminescence and defects creation processes in lead tungstate crystals. Tartu, 2007.
54. **Küllike Rägo.** Superconducting properties of MgB_2 in a scenario with intra- and interband pairing channels. Tartu, 2008.
55. **Els Heinsalu.** Normal and anomalously slow diffusion under external fields. Tartu, 2008.
56. **Kuno Kooser.** Soft x-ray induced radiative and nonradiative core-hole decay processes in thin films and solids. Tartu, 2008.
57. **Vadim Boltrushko.** Theory of vibronic transitions with strong nonlinear vibronic interaction in solids. Tartu, 2008.
58. **Andi Hektor.** Neutrino Physics beyond the Standard Model. Tartu, 2008.
59. **Raavo Josepson.** Photoinduced field-assisted electron emission into gases. Tartu, 2008.
60. **Martti Pärs.** Study of spontaneous and photoinduced processes in molecular solids using high-resolution optical spectroscopy. Tartu, 2008.
61. **Kristjan Kannike.** Implications of neutrino masses. Tartu, 2008.